UNIVERSIDADE FEDERAL DE SANTA CATARINA

CENTRO TECNOLÓGICO

PROGRAMA DE PÓS GRADUAÇÃO EM CIÊNCIA E ENGENHARIA DE MATERIAIS

Marcela Sagrilo Frizzo

Microwave-assisted hydrothermal synthesis of doped titanium dioxide quantum dots and its application in photocatalysis

Florianópolis

2021

Marcela Sagrilo Frizzo

Microwave-assisted hydrothermal synthesis of doped titanium dioxide quantum dots and its application in photocatalysis

Tese submetida ao Programa de Pós-Graduação em Ciência e Engenharia de Materiais (PGMAT) da Universidade Federal de Santa Catarina (UFSC) para a obtenção do título de doutor em Ciência e Engenharia de Materiais.

Orientador: Prof. Dr. João Batista Rodrigues Neto

Co-orientador: Prof. Dr. Dachamir Hotza

Florianópolis

2021

Marcela Sagrilo Frizzo

Microwave-assisted hydrothermal synthesis of doped titanium dioxide quantum dots and its application in photocatalysis

O presente trabalho em nível de doutorado foi avaliado e aprovado por banca examinadora composta pelos seguintes membros:

Dr. André Luiz da Silva
Universidade Federal de São Paulo

Prof. Valderes Drago, Dr.
Universidade Federal de Santa Catarina

Prof. Claudio Michel Poffo, Dr.
Universidade Federal de Santa Catarina

Certificamos que esta é a versão **original e final** do trabalho de conclusão que foi julgado adequado para obtenção do título de doutor em Ciência e Engenharia de Materiais.

_____

Coordenador do Programa de Pós-Graduação

_____

Prof. João Batista Rodrigues Neto, Dr.
Orientador

Florianópolis, 2021.

RESUMO

Nanocristais semicondutores coloidais, também conhecidos como pontos quânticos (PQs), têm atraído grande atenção por apresentarem interessantes propriedades dependentes do tamanho, devido ao efeito de confinamento quântico. Particularmente, os PQs de dióxido de titânio (TiO_2) apresentam propriedades dielétricas, ópticas e mecânicas exclusivas, bem como inúmeras aplicações potenciais, incluindo fotocatálise, revestimento óptico e células solares fotoeletroquímicas. Neste trabalho, PQs de TiO_2 foram sintetizados e avaliados como fotocatalisadores para a degradação do corante azo vermelho reativo (RR141) e do antibiótico tetraciclina. Os PQs foram produzidos utilizando tratamento hidrotérmico assistido por micro-ondas, de baixo consumo de energia e ecologicamente correto. Foram avaliados diferentes tempos de micro-ondas (10, 20, 30 e 60 min) e temperaturas (120, 140, 160, 180 ºC). Os dados de difração de raio-X (DRX) e espectroscopia de Raman indicaram anatase como a fase cristalina principal. As análises de DRX demonstram que há um aumento na componente interfacial conforme a temperatura de micro-ondas diminui, o que resulta em superfícies altamente energéticas e PQs super adsorventes. Os cristalitos de PQs de TiO_2 apresentaram um tamanho médio de ~ 5 nm, calculado pela Equação de Scherrer a partir dos espectros de DRX e confirmado por micrografias de transmissão eletrônica (MET). Como característica da redução do tamanho de partícula, os PQs apresentaram uma grande área de superfície específica (~290 $m^2 \cdot g^{-1}$), uma alta capacidade de adsorção e uma degradação rápida (~5 min) de 100% do corante azo RR141, utilizando comprimento de onda UV-B. Com o intuito de aumentar a fração da componente interfacial, melhorar a propriedade adsortiva e baixar o *gap* dos PQs foi realizada a dopagem dos mesmos com uma razão molar de 1, 2, 3% de Ca^{2+} e 1, 2, 3, 4% de La^{3+}. Como resultado, os PQs mantiveram a fase cristalina e tamanho de cristalito. As amostras dopadas com 1% de Ca^{2+} demonstraram um aumento significativo de área superficial específica (~412 $m^2 \cdot g^{-1}$), aumentaram a fração do componente interfacial de 60 para 64%, apresentaram absorção na região do visível e uma diminuição na energia do *band gap* de 3,03 para 2,72 eV, possibilitando a degradação do antibiótico tetraciclina utilizando lâmpada com comprimento de onda visível.

Palavras-chave: TiO₂, pontos quânticos, dopagem, micro-ondas, componente interfacial, adsorção, fotocatálise

RESUMO EXPANDIDO

SÍNTESE HIDROTERMAL ASSISTIDA POR MICRO-ONDAS DE PONTOS QUÂNTICOS SUPERADSORVENTES DE DIÓXIDO DE TITÂNIO DOPADOS PARA APLICAÇÃO EM FOTOCATÁLISE

Introdução

Nas últimas décadas, as energias limpas e renováveis têm se tornado alvo de pesquisas devido à alta dependência de combustíveis fósseis e aos altos níveis de poluição gerados pelo uso desses recursos. Os Processos Oxidativos Avançados (POAs) têm sido amplamente estudados como alternativa ou complemento aos processos convencionais de tratamento de efluentes, uma vez que os radicais hidroxila gerados pelo catalisador são altamente reativos, favorecendo a mineralização de poluentes. Dentre os materiais ambientalmente amigáveis, os PQs de TiO_2 podem ser considerados interessantes materiais absorvedores, com potencial aplicação em reações de fotocatálise devido sua proporção entre área de superfície e volume. Nesse sentido, os materiais nanoestruturados são formados por dois componentes, um cristalino com dimensões da ordem de alguns nanômetros que preserva a estrutura do cristal *bulk*, e outro denominado componente interfacial, que compreende vários tipos de defeitos (contornos de grão, interfase, limites, deslocamentos, etc). A fração de volume dos dois componentes é comparável, portanto, a alta densidade de interfaces e a grande fração de átomos presentes no componente interfacial se torna interessante, do ponto de vista, que é possível buscar novas características e/ou propriedades por meio de técnicas de modificação de superfície. Tais manipulações podem induzida pela incorporação de defeitos que podem transformar as propriedades físicas e químicas dos materiais para aplicações em tecnologias específicas. Recentemente, a rota hidrotermal assistida por micro-ondas ganhou atenção para a síntese de PQs de TiO_2 devido ao menor tempo de reação, rápida transferência de calor e energia, entendido como um processo ecológico, que requer menor consumo de energia do que os processos convencionais de aquecimento e aumento do rendimento do produto. O tratamento térmico assistido por micro-ondas fornece uma forma de aquecimento mais eficiente em comparação com a síntese hidrotérmica convencional, pois o calor é direcionado imediatamente para a

solução enquanto que, em um forno convencional, o calor precisa ser dissipado do forno para o reator e depois para a solução real. Trata-se, portanto, de um método mais rápido que costuma levar alguns minutos, em comparação com o hidrotermal, que pode durar até várias horas.

Objetivo

Este trabalho propõe a síntese, a dopagem e a caracterização de PQs de TiO_2 a fim de explorar a propriedade de adsorção dos mesmos. Os pontos quânticos foram aplicados em reações de fotocatálise para a degradação do corante azo RR141 e do antibiótico tetraciclina. A primeira etapa do trabalho consistiu em definir os parâmetros ótimos de tempo e temperatura do tratamento térmico assistido por micro-ondas. Para tanto, o material foi caracterizado microestruturalmente e foram realizados ensaios de adsorção e fotocatálise, do corante RR 141 utilizando comprimento de onda na região ultravioleta (UV-B). Com base nos melhores resultados, e definidos os parâmetros de tempo e temperatura, partiu-se para a segunda etapa do trabalho que consistiu em avaliar a influência da dopagem, com íons de lantânio (La^{3+}) e cálcio (Ca^{2+}), em relação à fração da componente interfacial, a fim de aumentar os defeitos na estrutura superficial dos pontos quânticos, tornando-os mais adsorventes e capazes de diminuir a taxa de transferência de carga eletrônica entre a banda de condução e a banda de valência, permitindo, desta forma, que pudesse ser utilizado comprimento de onda na região do visível para as reações de fotodegradação do antibiótico tetraciclina.

Metodologia

A síntese dos pontos quânticos se deu pela hidrólise, em uma solução aquosa (18.2 MΩ cm^{-1}, ultrapura Milli-Q) em meio ácido (HNO$_3$, 65 %, Vetec) do precursor tetraisopropóxido de titânio (TTIP97%, Sigma) sob agitação contínua a 600 rpm e temperatura ambiente, com razões molares de H_2O: Ti^{4+} =110:1 e H^+: Ti^{4+}= 0.35. Após 30 minutos de agitação, a reação foi transferida para um vidro borossilicato, contendo 20 mL de solução, então fechado e colocado um sistema de reator de micro-ondas (Monowave 300, Anton Paar). O sistema operou com uma frequência de 2.45GHz e potência máxima de 850W, o qual a pressão foi modulada dependendo da temperatura. Estipulou-se uma rampa de aquecimento de 5 minutos. Inicialmente, testou-se 10, 20, 30 e 60 minutos à 180°C. Por fim, as amostras foram lavadas 3 vezes com água

destilada e centrifugadas a 4500 rpm, secas à 100°C, maceradas e caracterizadas. Definiu-se 10 minutos como o melhor tempo para o tratamento térmico. A etapa seguinte foi a variação da temperatura e para tanto testou-se 180, 160, 140 e 120°C. Seguido das caracterizações e com base nos resultados de menor tamanho de cristalito, maior área de superfície específica (BET), maior porcentagem de componente interfacial, melhor desempenho nos testes de adsorção do corante RR14 foram fixados os parâmetros ótimos de tempo e temperatura em 120°C e 10 minutos. Para a dopagem dos pontos quânticos, Ti^{4+} foi substituído em proporções molar de 1,2,3 e 4% por La^{3+} e 1, 3 e 5% de Ca^{2+}. O procedimento experimental foi o mesmo para a síntese dos pontos quânticos, porém o nitrato de lantânio hidratado (LaN_3O_9 99.9%, Sigma-Aldrich) foi adicionado à solução aquosa ácida e mantido sob agitação contínua por 10 minutos, previamente à adição do precursor. O mesmo se deu para o nitrato de cálcio tetrahidratado ($Ca(NO_3)_2.4H_2O$ P.A, Neon). Após 30 minutos da etapa de agitação, as reações foram transferidas para o reator de micro-ondas para o tratamento térmico a 120°C por 10 minutos, seguidas das etapas de lavagem, centrifugação, secagem e maceração para posterior caracterização e ensaios de adsorção e fotocatálise. O procedimento experimental está esquematizado no Apêndice A.

Resultados e Discussão

Os espectros de padrões de DRX das amostras tratadas termicamente com 10 minutos em diferentes temperaturas (120, 140, 160 e 180 ºC) apontam anatase como fase cristalina majoritária. A largura a meia altura (FWHM) dos padrões de DRX foram utilizadas para calcular os tamanhos de cristalito por meio da equação de Scherrer. Com a diminuição da temperatura de síntese, houve um aumento da fração do componente interfacial (52, 55, 56 e 60 %), ocorre também uma diminuição no tamanho médio do cristalito das amostras (6.2, 5.5, 5.1, 5.0 nm) e um aumento das áreas de superfície específicas (245, 253, 257 e 292 $m^2.g^{-1}$). Para confirmar o efeito da alta temperatura nas características estruturais dos PQs, o tratamento térmico a 650 ºC foi realizado na amostra sintetizada em 120 ºC. Pela análise do padrão de DRX, o material tornou-se altamente cristalino com a nucleação da fase rutilo. Além disso, o componente interfacial foi fortemente reduzido (~ 5%). Para todas as amostras a taxa de adsorção do corante RR141 é maior nos primeiros 5 minutos. Quanto mais alta a temperatura de tratamento térmico, menor o desempenho de adsorção. Na amostra sintetizada a 120 ºC,

65% do RR141 foi adsorvido nos primeiros 5 min em comparação à amostra de 180 ºC, que atingiu apenas 29%. Para o desempenho fotocatalítico foram comparadas reações com e sem adsorção prévia, respectivamente. Quando a lâmpada UV-B é ligada desde o início do processo, todas as amostras apresentam comportamento semelhante levando 15 minutos de irradiação para degradar 100% do corante RR141. Com o processo de adsorção prévio, em apenas 5 min 100% do corante RR141 foi degradado pela amostra tratada à 120 ºC. Este comportamento pode ser explicado pela alta taxa de adsorção dos corantes na superfície dos pontos quânticos, pois quando a lâmpada é ligada, a quantidade de corante adsorvido é rapidamente degradada. Assim, as amostras que apresentaram melhor desempenho em adsorção/fotocatálise, foram reutilizados em 3 ciclos, para a degradação do corante RR141. O processo de adsorção diminui a eficiência após cada ciclo, provavelmente devido a uma superfície mais saturada. Portanto, a fotocatálise leva mais tempo para degradar o corante RR em um novo ciclo. Não houve alteração da fase cristalina para as amostras e os tamanhos de cristalitos ficaram entre 4,9-5,0. Com o aumento da porcentagem de dopantes houve um aumento da fração do componente interfacial (de 60 para 64%) e consequente diminuição da fase cristalina. Tais variações podem ser decorrentes de defeitos introduzidos no sistema por meio da dopagem. Esses mecanismos podem elucidar as diferenças entre os valores de áreas superficiais específicas para um mesmo tamanho de cristalito. O raio iônico do Ca^{2+} (0,100 nm) e La^{3+} (0,103 nm) são significativamente maiores do que Ti^{4+} (0,061 nm). Somando suas diferentes valências com baixa solubilidade na rede cristalina, esses íons de dopagem são frequentemente segregados para os contornos do grão. Desta forma, a energia livre do contorno do grão pode ser reduzida. Isso esclarece porque o excesso de dopante diminui a área de superfície específica. A amostra com 1 % de Ca^{2+} apresentou o melhor resultado de área superficial especifica (412,1 $m^2.g^{-1}$) comparando a 1 % de La^{3+} (309,51 $m^2.g^{-1}$), essas diferenças podem ser atribuídas as interações entre as ligações Ti-O-Ca e Ti -O-La nas regiões limítrofes da estrutura atômica. Devido a diferença de eletronegatividade entre os dopantes as interações entre os átomos de Ti-O-Ca podem se dar com diferente intensidade comparada às ligações Ti-O-La. Podendo haver diferentes desequilíbrios de cargas. O mecanismo de compensação de cargas induz a formação de vacâncias de oxigênio e titânio. Além disso, se um cristal é submetido a tensão de tração ou conforme o comprimento da ligação química aumenta e a constante de força permanece a mesma, a frequência vibracional diminui e um desvio para o vermelho é observado no espectro Raman. O melhor resultado dos testes de

adsorção do antibiótico tetraciclina foi para a amostra dopada com 1% de Ca^{2+}, devido sua elevada área de superfície. Os valores de gap óptico TiO_2 puro ficou em 3,03 eV. As amostras com 1 e 3% de Ca^{2+} alcançaram o E_{bg} 2,72 eV, tornando-as excitáveis com a radiação de menor energia e também apresentam melhor atividade fotocatalítica em relação ao restante, o que leva à conclusão de que a quantidade de tetraciclina adsorvida na superfície e a diminuição de o gap induz a reação de fotocatálise.

Considerações Finais

Em resumo, apresentamos pontos quânticos altamente homogêneos de TiO_2 e TiO_2 dopados com Ca^{2+}/La^{3+} via síntese hidrotermal assistida por micro-ondas, em uma temperatura mais baixa (120 °C) e um tempo mais curto (10 min) do que nos processos tradicionais. Os padrões de DRX mostraram anatase como fase cristalina principal e um aumento na fração do componente interfacial conforme a temperatura de micro-ondas diminui, resultando em uma superfície altamente energética e com propriedades de adsorção. As amostras dopadas com 1 mol% de Ca^{2+} resultaram em materiais com alta área de superfície (412,19 $m^2.g^{-1}$), e um aumento na fração da componente interfacial (64%). Além disso, ampliaram o espectro de absorção para comprimentos de onda na região do visível, diminuendo a energia do *band gap* de 3.02 eV (TiO_2 puro) para 2,72 eV), tornando possível a utilização de luz visível para degradação de 96% do antibiótico tetraciclina nas reações de fotocatálise. No geral, a tecnologia usada nesta pesquisa fornece suporte técnico para a preparação de pontos quânticos de TiO_2 e TiO_2 dopados como matéria-prima para diversas aplicações, além de uma base científica para a produção industrial desses fotocatalisadores.

ABSTRACT

Colloidal semiconductor nanocrystals, also known as quantum dots (QDs), have attracted great attention since they have interesting size-dependent properties due to the quantum confinement effect. Particularly, titanium dioxide (TiO_2) QDs present unique dielectric, optical, and mechanical properties as well as numerous potential applications including photocatalysis, optical coating, and photoelectrochemical solar cells. In this work, TiO_2 QDs were synthesized and evaluated as photocatalysts for the degradation of reactive red azo dye (RR141) and tetracycline antibiotic. QDs were produced by a low-energy and eco-friendly microwave-assisted method. Different microwave times (10, 20, 30, and 60 min) and temperatures (120, 140, 160, 180 ºC) were evaluated. Raman and X-ray diffraction data detected anatase as the major crystalline phase. XRD also indicated an increase in the interfacial component as the microwave temperature decreases, resulting in highly energetic surface and super adsorptive QDs. TiO_2 crystallites presented an average size of ~5 nm as calculated from XRD spectra and confirmed by TEM micrographs. As a feature of the particle size reduction, the QDs presented a large specific surface area (~290 $m^2.g^{-1}$), a high adsorption capability, and a fast (~5 min) 100% degradation of RR141 using UV-B wavelength. In order to increase the interfacial component fraction and improve the adsorptive property and band gap of the QDs, they were doped with 1, 2, 3% molar ratio of Ca^{2+} and 1, 2, 3, 4 % molar ratio of La^{3+}. As a result, the QDs maintained the crystallite size and the sample doped with 1% of Ca^{2+} presented a high specific surface area (~412 $m^2.g^{-1}$), increased the interfacial component from 60 to 64% and showed a decrease in bandgap from 3.02 to 2.72 eV, making it possible to carry out the degradation of tetracycline antibiotic using UV-vis wavelength.

Keywords: TiO₂, quantum dots, doping, microwave, interfacial component, adsorption, photocatalysis.

LIST OF FIGURES

LIST OF TABLES

LIST OF ABREVIATIONS AND SYMBOLS

TiO_2 – Titanium dioxide

QDs - Quantum dots

AOPs - Advanced Oxidative Processes

VB – Valence band

CB – Conduction band

BG - Band gap

OM - Molecular Orbital

e^- - Electron

h^+ - electron hole

eV – eléctron volt

GHz- Gigahertz

rpm – rotation per minute

E_{bg} - Band gap energy

·OH - Hydroxyl radical

CO_2 - Carbon dioxide

$H_2O•$ - Hydroperoxy radical

XRD - X-ray Diffraction

TEM- Transmission Electron Microscopy

NIR - Near infrared region

PCE - photo conversion efficiency

QDSSCs - Quantum-dot-sensitized solar cells

DSSC- Dye-sensitized solar cell

SSA - Specific surface area

HNO$_3$- Nitric acid

MO - Methyl Ora

RR - Reactive red

UV-B -Ultraviolet

UV-Vis – Ultaviolet visible

FWHM- Full width at half maximum

σ_i - Interfacial energy

σ_0 - Interfacial energy of the undoped material

Γ_i - Solute excess at the interface

ΔH_{seg} - Enthalpy of segregation

pH -Potential of hydrogen

TABLE OF CONTENTS

Chapter 1 - Introduction and Objectives

1.1 Introduction

The large demographic growth and industrial expansion is responsible for an increasing waste generation of different compositions and complexities, comprising the families of dyes, pesticides, herbicides, pharmaceuticals, cosmetics, phenolic compounds, toxins, among others, which are not treated by conventional effluent techniques. These products are classified after their disposal as emerging pollutants, which in most cases can be water-soluble, recalcitrant and carcinogenic[1].

Advanced Oxidative Processes (AOPs) have been extensively studied as an alternative to, or complement to, conventional wastewater treatment processes, since the hydroxyl radicals generated by the catalyst are highly reactive, favoring the mineralization of emerging pollutants[21-23]. TiO_2 photocatalysts are materials that exhibit excellent absorption behavior toward organic compounds in wastewater due to their outstanding properties including nontoxicity, high photocatalytic degradation ability, and excellent thermal and chemical stabilities[14-15].

Progress in nanotechnology has been leading to the development of new types of photocatalysts. Photocatalysts of the same material in nano scale show properties quite different from the bulk state. This can be attributed to the effect of surface area and quantum confinement. Quantum dots (QDs) have been intensively studied because of their high surface area to volume ratio, which leads to a high fraction of particles, and therefore a high fraction of active sites available to react on the catalyst surface. Furthermore, dependence on the size of the nanocatalyst makes it possible to tune the wavelength at which the material absorbs the energy to the bandgap, with an objective to harness solar energy to degrade the organic compounds[19, 32-35].

In this regard, nanostructured materials are composed of crystalline core, that preserves the structure of a bulk crystal, and interfacial component, which comprises several types of defects, such as grain boundaries. The volume fraction of the two components is comparable, and the high density of interfaces and the high number of atoms present in the interface allows its manipulation, for example, introducing new surface modification or via thermic treatment or doping, leading to the possibility of tuning the physical properties for specific technology[39-43].

Several routes have been explored to synthesize QDs for the degradation of organic molecule. Microwave synthesis is an environmentally friendly method that offers high

homogeneity and yield in short synthesis times. Therefore, microwave synthesis produces small and homogeneous nanoparticles, due to the high reaction rate and volumetric heating[57,63-66].

In this work, we report a facile and safe method to prepare pure and Ca^{2+}/La^{3+} doped TiO_2 QDs with a high specific surface area and highly adsorptive via microwave-assisted hydrothermal process. Manipulation of interfacial component of QDs by the adjustment (time and temperature) of microwave parameters and doping was conducted to optimize their photocatalysis efficiency. The adsorption process and degradation of reactive red azo dyes and tetracycline antibiotic were evaluated. Structural, morphological and electronic properties, as well as recycling features were studied.

1.2 Research Objectives

This work aimed to develop, by microwave-assisted hydrothermal synthesis, doped and undoped titanium dioxide quantum dots with adsorbent properties for photocatalysis application.

The specific objectives were:

- Evaluate microwave-assisted hydrothermal treatment time/temperature parameters and characterize the samples;
- Apply samples to adsorption and photocatalysis tests for degradation of reactive azo red dye (RR 141);
- Define the synthesis parameters, by doping with La^{3+} and Ca^{2+} in different proportions, as well as the improvement of characterization techniques on the surface of QDs.
- Apply samples to adsorption and photocatalysis tests for degradation of tetracycline antibiotics using a visible light.

1.3 Thesis structure

This thesis is structured in five chapters. Chapters 1 and 2 comprises, respectively, the introduction and a literature review of relevant topics related to this work. Research chapters are presented in chapter 3 and 4. Each one is divided into sections: introduction, materials and methods, results, discussion and conclusions. References are merged at the end of the document. Chapter 3 was based on the manipulation of interfacial component of QDs by the adjustment (time and temperature) of parameters of microwave synthesis of TiO_2 QDs to optimize their adsorption and photocatalysis efficiency. The adsorption process and degradation of reactive red azo dyes were evaluated. Structural and morphological properties, as well as recycling features, are also presented. Chapter 4 shows pure and Ca^{2+}/La^{3+} doped TiO_2 QDs synthesized via hydrothermal microwave treatment at 120 °C for 10 minutes to incorporate more defects in the surface structure of the quantum dots, turning them more adsorbent, making it possible to use wavelength in the region of visible for photodegradation reactions of the antibiotic tetracycline. Finally, in chapter 5 the general conclusion and an outlook for future works are presented.

Chapter 2 - Literature review

2.1 Titaniun Dioxide (TiO$_2$) and heterogeneous photocatalysis

Among the semiconductor materials explored, TiO$_2$ has some advantages that highlight its use in the market: low toxicity, photostability, chemical stability against pH variations, resistance to acids and, when compared to other oxides, a high photocatalytic activity[1].

TiO$_2$ belongs to the family of transition metal oxides and the three most known polymorphic structures are anatase, rutile, and brookite, illustrated in Figure 1. The anatase phase has a tetragonal structure and is preferred among other Fermi level polymorphs for applications in solar cells and photocatalysis due to its greater electronic mobility and low dielectric constant[2]. The increased photoreactivity is due to the being slightly higher, having a low capacity to adsorb oxygen and a greater degree of hydroxylation. However, the phase is metastable and irreversibly converted to the rutile phase. Rutile is also formed by a tetragonal structure that contains 6 atoms per unit cell and is stable at most temperatures and pressures up to 60 kbar[3-5]. Brookite, on the other hand, belongs to the orthorhombic crystalline system, composed of a more complex structure, has a larger volume and lower density than the other polymorphs, and due to its synthesis difficulty, it is poorly used in scientific experiments[6].

Figure 1-Polymorphic structures of TiO$_2$
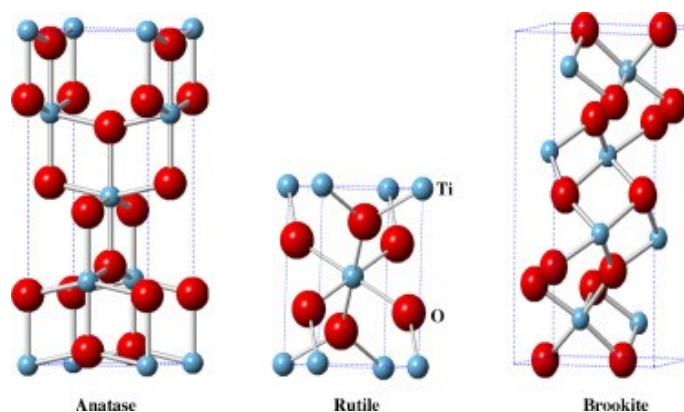
Source: Etacheri et al. (2015)[7]

The factor that determines the electrical properties of a solid is the distribution of its electrons, and according to the Molecular Orbital (OM) theory, all valence electrons occupy molecular orbitals that are delocalized over the entire molecule, i.e., do

not belong to any particular bond. The molecular orbital is a wave function and is formed by the addition/superposition of atomic orbitals that belong to the valence layer of the atoms of the molecule[8]. Figure 2 illustrates the superposition of the *s* and *p* orbital, when *p* orbits have higher energies than *s* orbitals, the *p* band will be higher and there might be a space between the bands, an energy gap, called band gap, which does not correspond to any orbitals. However, depending on the material, this space can be very small, so *s* and *p* bands overlap, as in the case of magnesium[9].

Figure 2 - Illustration of the superposition of the s and p orbitals that give rise to the s and p bands
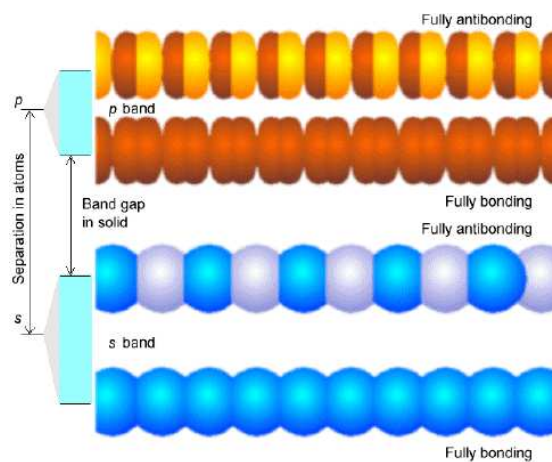
Source: Aktins and Paula (2008)[9]

TiO$_2$ energy level diagram, which combines the molecular orbital theory with that of the crystalline field, is shown in Figure 3. The valence band of anatase TiO$_2$ is comprised of O p$_\pi$ (higher energy region), p$_\sigma$ and p$_\pi$ (intermediate energy region), and pσ (lower energy region). In contrast, the conduction band, which is more external, energetic and away from the nucleus has empty spaces is comprised of Ti 3d and 4s, and the lower energy regions of the conduction band are constructed by the degenerate e$_g$-like and threefold t$_{2g}$-like states resulting from the crystal field splitting of Ti 3d[11].

For electrons to move freely from the valence band to the conduction band they need to reach energy greater than the band gap energy to "jump". This energy is provided in the form of radiation, associated with a wavelength. The wavelength required to activate the catalyst must be equal to or less than that calculated by the Planck equation[10,11].

$$\lambda = \frac{hc}{E_{bg}} \qquad (1)$$

Where E_{bg} is the band gap energy (eV), h is Planck's constant ($4,136 \times 10^{-15}$ eV.s), c is the speed of light ($2,998 \times 10^8$ m/s) and λ is the wavelength (nm). The band gap of anatase and rutile is equivalent to 3.2 and 3.0 eV at 388 and 413 nm, respectively. When the wavelength affects the semiconductor, the electrons (e^-) from the valence band jump to the conduction band, creating positive (h^+) holes (electron/hole) in the valence band[12,13].

Figure 3 - TiO$_2$ energy level diagram and structure of valence and conduction bands
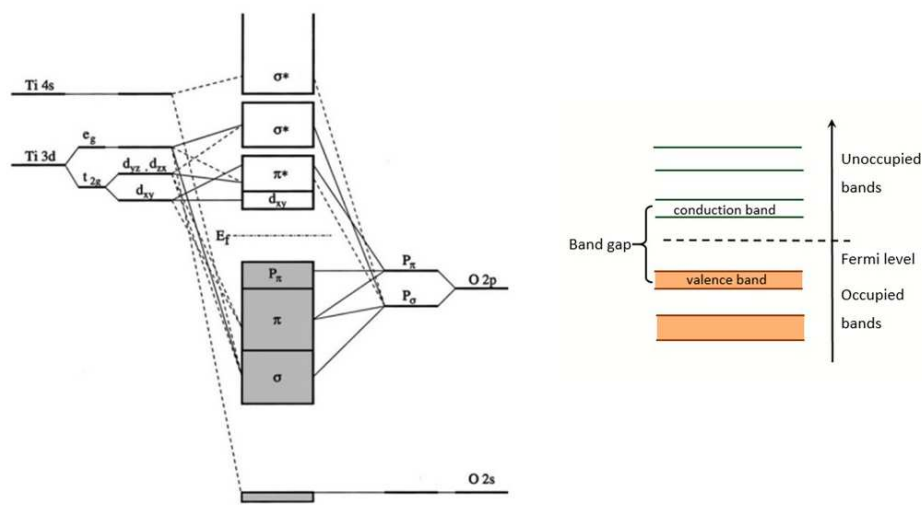
Source: Zhao et al. (2008)[11]

In a semiconductor with a wide band gap, valence electrons cannot jump into the conduction band without an external energy, the photoexcited state of in semiconductor is generally unstable and can easily break. TiO$_2$ remains highly stable, even when photoexcited. This is one of the reasons that contributes for anatase to play a better role in photocatalysis, as it has slower charge recombination and greater electron mobility[14,15].

One of the most studied applications of TiO$_2$ is its photocatalytic activity, which enables the degradation of a wide variety of toxic organic pollutants into less harmless substances: An example is Advanced Oxidation Processes (AOPs) with UV irradiation and titanium dioxide as a photocatalyst gaining increasing acceptance as an effective method of wastewater treatment[16-20].

Advanced Oxidative Processes (AOPs) have been extensively studied as an alternative or complement to conventional wastewater treatment processes, since the hydroxyl radicals generated by the catalyst are highly reactive, favoring the mineralization of emerging pollutants. AOPs are based on the use of highly oxidizing species to promote a more effective degradation of the pollutant to be treated. It comprises a set of techniques based on the generation of free radicals, mainly the hydroxyl radical ($\cdot$OH), which under certain conditions would be capable of transforming most organic contaminants into carbon dioxide (CO_2), water and inorganic salts, which proves to be a method for water purification that fits in the context of "Green Chemistry"[21-23].

Advanced degradation processes are divided into homogeneous systems, where there is no solid-state catalyst, it is dissolved in the solution, forming a single phase; and heterogeneous systems, which differ from homogeneous ones due to the presence of inorganic catalysts (semiconductors)[24]. Fujishima and Honda achieved for the first time, in 1972, the photoelectrochemical water splitting from light irradiation without electrical energy using *n*-type TiO_2 electrode as anode and Pt as cathode in an electrochemical cell[25]. This discovery attracted worldwide attention and triggered a series of research, especially after the oil crisis in 1973, since water splitting into oxygen and hydrogen with minimal energy consumption, through sunlight, would allow a process of renewable sustainable and non-polluting pathways. Thus, with the principles and measures carried out from the photoelectrochemical studies, extensive research in heterogeneous photocatalysis has been developed.

In this technique, the surface generation of oxi-reductive sites occurs through the electronic excitation of semiconductors. In Figure 4 it is possible to observe a schematic representation of a semiconductor photoactivation. This mechanism works with irradiation, that leads to electron transfer (e^-) from the valence band (VB) to the conduction band (CB), creating a hole (h^+) in VB. Oxidation-reduction reactions are initiated with the formation of the e^-/h^+ pair (i.e., excitons) inside compounds. Such compounds are later adsorbed on the surface of the photocatalyst. According to related works[26], reagents can be transferred to the photocatalyst surface by different processes, as described below:

1. Electronic reactions involving:

    (a) adsorption of reagents;

    (b) absorption of photons on the surface of catalysts;

(c) exciton formation;

(d) transfer of exciton to reaction sites of photocatalysts surface.

2. Surface chemical reactions including:

(a) reaction among adsorbed species.

3. Mass transfer involving:

(a) desorption;

(b) removal of products.

Figure 4 - Illustration of a semiconductor photoactivation mechanism
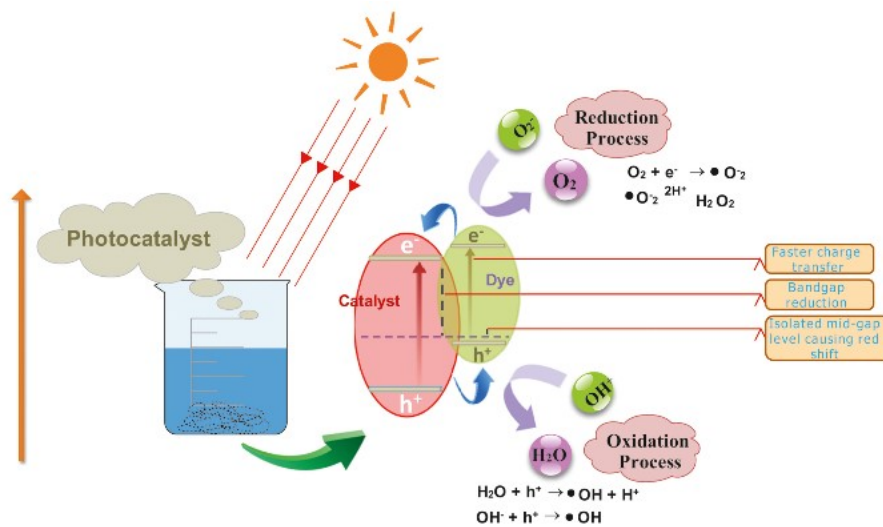
Source: Ikran et al. (2012)[26]

The general mechanism of TiO_2 reactions in heterogeneous photocatalysis[26-28] is characterized by different steps. Photocatalytic activity is initiated with the absorption of photon hv1 with an energy equal to or greater than the band gap of TiO_2 (~ 3.2 eV for the anatase phase) (Equation 2). This creates an electron-hole pair (e^-/h^+) on the surface of the semiconductor, which induces the excitation of an electron into the conduction band while a positive hole is created in the valence band.

$$TiO_2 \xrightarrow{hv} e^-_{bc} + h^+_{bv} \qquad (2)$$
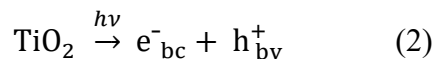
Equation 3 shows electrons generated by photon's irradiation react with O_2 and are converted to superoxide radical as $O_2^{\bullet-}$

$$e^- + O_2 \longrightarrow O_2^{\bullet-} \qquad (3)$$
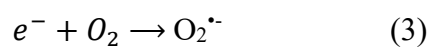
Subsequently, equation 4, the reaction of superoxide radicals $O_2^{\bullet-}$ with water produces oxidizing agents i.e. hydroperoxy ($H_2O\bullet$) and prevents recombination of the e-

/h+ pair, also generating additional hydroxyl radicals (OH·) needed for the decomposition of organic pollutants.

$$\bullet\, O_2^- + H_2O \rightarrow HO_2^\bullet + OH^\bullet \qquad (4)$$
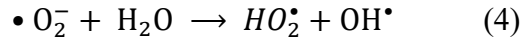
At the same time, Equations 5 and 6, water on the surface of the photocatalyst may trap in these holes generated by irradiation and produce hydroxyl radicals (OH·):

$$h^+ + OH^- \rightarrow HO_{ads}^\bullet \qquad\qquad (5)$$

$$h^+ + H_2O \rightarrow HO^\bullet + H^+ \qquad\qquad (6)$$
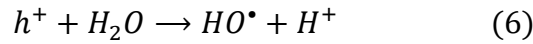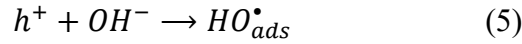
Finally, CO_2 and H_2O are produced by the oxidation of organic molecules as Equation 7.

$$O_2 + \text{Organic} + HO^\bullet \xrightarrow{h\nu} \text{products } (CO_2 + H_2O) \qquad (7)$$
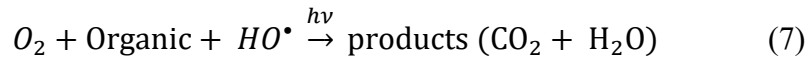
Furthermore, the photocatalytic activity of the nanocatalyst is affected by even slight recombination of the electron-hole pair that may eventually be lost (Equation 8).
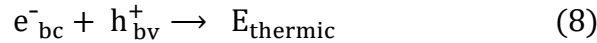
$$e^-_{bc} + h^+_{bv} \rightarrow E_{thermic} \qquad\qquad (8)$$

Many variables can affect the efficiency of a photocatalyst, such as a particle/grain size, specific surface area, crystallinity, light intensity, catalyst concentration and adsorption capacity[17]. To understand the influence of these variables on catalysis, investigations on nanostructured materials have increasingly grown. The reduction in particle and/or grain size is followed by an increase in surface area and an enrichment of surface defects (edges, corners, and faces of the crystal) in nanoparticles when compared to their bulk counterparts. These effects eventually change the electronic microenvironment and the electric charge transfer[29]. Among the low dimensional structures, the quantum dots (QDs) demonstrate extraordinary properties due to the confinement of particles in all three dimensions. The higher surface area to volume ratio of QDs made them excellent nanophotocatalysts, particularly for environmental applications, such as water and air purification[30,31].

2.2 Quantum dots semiconductors

Among nanoscale materials, quantum dots (QDs) are three-dimensional structures with sizes between 1 and 10 nm, defined as particles smaller than the exciton Bohr radius. They have charge carriers (electrons and holes) in a state of strong confinement[19,32].

Quantum confinement leads to the formation of discrete levels in the valence and conduction bands, which present an intermediary behavior between crystals and

isolated atoms. The discrete spectrum of energy states of this material is similar to the energy spectrum of individual atoms. Because of this similarity, QDs are called "artificial atoms"[33,34].

The confinement of pairs of electrons and holes in three dimensions leads to an increase in energy between the valence band and the conduction band (forbidden band energy – band gap) of the materials, according to their size decrease the greater the confinement of charge carriers and the greater the band gap energy[29,34,35] as illustrate in Figure 5. Consequently, the gap and emission properties can be fine-tuned just by controlling the size of these materials. The unique properties of QDs make it possible to overcome the limitations that arise from using bulk materials.

Figure 5 Schematic representation of emission spectra depending on the size of QDs relating to their band gap energy (Eg), considering three-dimensional confinement
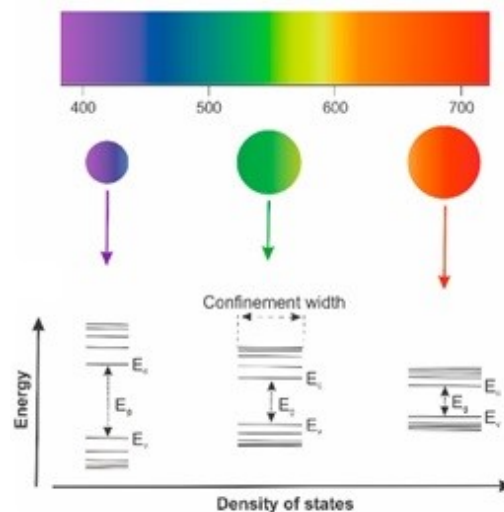
Source: Galstyan V. (2021)[109]

Due to their small size, quantum dots have special optics characteristics, a wide spectrum of excitation, allowing a greater choice of wavelengths for their excitation; high photostability, that enables excitation during long periods without their degradation; possibility of joining with organic molecules without losing the photoluminescence; adjustable chemical activity and excellent selectivity. All these characteristics make them excellent candidates for photocatalysis, as already reported elsewhere[19,32,36-38].

2.3 New properties *vs* structure of nanomaterials

In materials science, advances have been reported either by developing and applying new research methods, or by manipulating materials searching new characteristics and/or structural properties. The lowest free energy state of a solid at low temperature is the perfect crystal, i.e., an organized or nearly organized three-dimensional array of atoms. Figure 6 shows a schematic illustration of a hard sphere two-dimensional model of a hypothetical nanocrystalline material[39,40]. There are two types of atoms in the nanocrystalline structure: crystal atoms with neighboring lattice configuration and boundary atoms with a variety of interatomic spacings.

Figure 6 - Schematic representation of two-dimensional model of nanocrystalline material. Atoms in the crystalline region are indicated as black circles, while those in the interface regions are presented as open circles
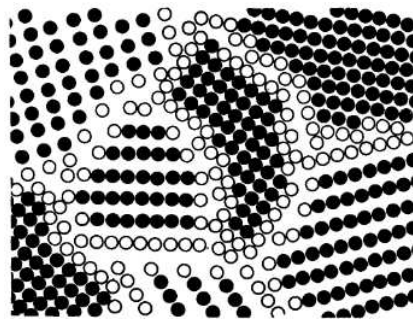
Source: Gleiter (2000)[40]

When the crystalline material is reduced to a few nanometers, the fraction of the volume occupied by the interfaces (interfacial component) becomes comparable to the volume of the ordered crystalline core (Figure 7). The interfacial component consists of many boundaries (typically 10^{19} cm)[40]. As the structures of these boundaries are all different, the interface component is the sum of all boundary structures. For example, considering a nanocrystalline material of randomly oriented crystallites with diameters of 5 nm, and interface thickness 1 nm, the system will contain about 10^{19} interfaces per cm^3 occupying a volume fraction of approximately 40 %[39-43].

Figure 7- Interface properties become increasingly dominant as the particle size is reduced
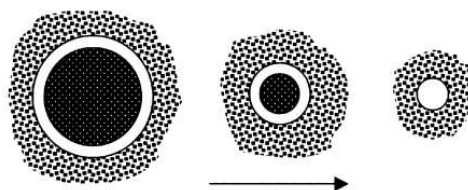
Source: Lewis (2004)[44]

The atomic displacements associated with the incorporation of defects significantly alter the atomic density and coordination in the interfacial component to about 15 to 30 % less than that of the crystalline core. Consequently, the core structure of the grain boundaries depends on interatomic bonding forces and boundary crystallography (e.g., the disorientation between both crystals, the slope of the boundaries and the translational position of one crystal relative to the others). Therefore, there is a variety of interfacial component structures in different materials.

For nanocrystalline materials, the processing of materials with different structures and atomic properties is focused on atomic arrangements in the core of defects, such as grain boundaries, interphases, or displacement. In the last decades, studies on the manipulation of solids defects have revealed significant properties. Such manipulations can be divided into two groups; (1) manipulation by the thermal disorder of the crystal structure followed by freezing in the disordered state through quenching; (2) induced by the incorporation of defects such as voids, displacements, grains, or interface boundaries[39-41].

Due to the fact that nanomaterials present such a pronounced phase, in this work we seek to manipulate the fraction of the interfacial component, to study the variations in material properties. We believe that techniques such as doping can interfere with the properties, as the insertion of ions increases the material's defects and, consequently, can contribute to the interfacial phase.

2.4 Doping

Sun-powered photocatalysis is an emerging, renewable and sustainable approach in environmental remediation to mitigate organic pollutants from wastewater. To increase the efficiency of a photocatalyst system, it is necessary for the photocatalyst to degrade pollutants using visible and/or solar light irradiation[7,47].

Therefore, it is necessary to optimize the synthesis of the catalyst to obtain nanoparticles with large surface area available for reactions. The use of the sunlight spectrum, whose doping is preferred because it adjusts the band gap for absorption of the light to the near infrared region (NIR) results in improved photocatalytic proficiency[48].

The effect of metallic ionic dopants on photocatalytic activity is complex. The induced alteration in the photocatalytic activity is made from a sum of modifications,

such as: the light absorption capacity of the photocatalyst; adsorption capacity of substrate molecules on the catalyst surface; and the interfacial charge transfer rate[49-51].

TiO_2 particles can be doped in substitutional or interstitial sites with different ions. The dominant parameters include the character and concentration of the dopant, the synthesis method and the heat treatment[52-54].

Doping of n-type semiconductors is obtained by dissolving cations with higher valences than Ti^{4+} (Nb^{5+}, Ta^{5+}, Sb^{5+}) in the TiO_2 lattice, while p-type doping is obtained by cations with valences lower than those of Ti^{4+} (Al^{3+}, Cr^{3+}, Ca^{2+}, Ln^{3+}). The inhibition effect is attributed to an increase in the electron-hole recombination rate. More precisely, p-type dopants act as acceptor centers, which trap electrons and once negatively charged, attract holes, thus forming recombination centers. In contrast, n-type dopants act as donor centers. Increasing the concentration of conducting electrons, however, in some cases, can favor the recombination of e^-/h^+ [15,56,57].

Although, when dopant is little immiscible in the lattice of the crystallites, for example, when the ionic radius of the dopant is bigger than that of the host, it frequently segregates to the grain boundary[40,58,59]. As shown in Figure 8, the black holes are the dopants ions segregated on the interfacial component. Segregation ions to the grain boundaries leads to a decrease in the free energy of the system, stabilizing grain growth.

Figure 8 Schematic illustration of dopants ions segregates to the grain boundaries
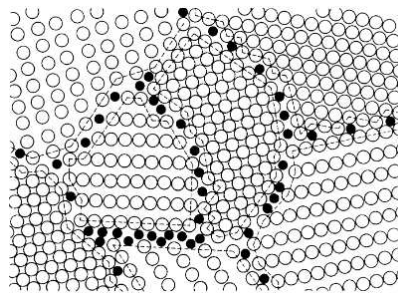
Source: Gleiter (2000)[40]

If segregation of the ions occur and there is an excess dopant, it can remain on the semiconductor surface and also change the adsorption patterns, as reported by da Silva et al. (2020)[60] in TiO_2 doped with alkaline-earth ions.

Alkaline earth metals such as calcium (Ca) and sodium (Na) are widely used as mordants for fixing dyes to fabrics. Concerning that, Weixin Li et al. (2014)[145] and Prabavathy et al. (2019)[146] doped Ca over TiO_2 to DSSC and observed that doping with Ca increased the photovoltaic performance of the cell due to an increase in dye

concentration in the photoelectrode. Furthermore, optical studies inferred that the band gap of the TiO_2 film decreased from 3.08 eV to 2.75 eV with increasing Ca doping.

Following this line, Rafieh et al. (2021)[61] synthesized pure and Ca and La doped TiO_2 nanoparticles via sol gel method to increase the adsorption capacity of the N719 dye for application on dye-sensitized solar cell (DSSC) anode. Since dopant types will have a different influence on the characteristics of a material, they should be selected based on the changes that must be achieved. For example, to improve the photocatalytic activity of TiO_2, lanthanum (La) compounds have been previously used and demonstrated to be advantageous in improving the degradation of the photocatalytic dye[56]. Doping TiO_2 with La^{3+} ions has shown to improve the adsorption rate of organic compounds that are associated with the formation of oxygen vacancies. When La^{3+} ions are introduced into TiO_2, they scavenge oxygen to form La-O bonds that have a stronger chemical binding energy compared to Ti-O bonds. As a result, oxygen gaps can be formed, which influence the level of dye adsorption and charge transport within the material[125].

Based on presented, it was possible to observe that doping with Ca and La can lead to an adsorption increase of TiO_2. Based on these effects, we chose to use these two elements as dopants for this work.

2.5 Microwave-assisted hydrothermal route

A well-defined and controlled preparation method is of great importance to produce nanoparticles with properties that define them as good photocatalysts.

Recently, microwave-assisted hydrothermal route has gained attention for the synthesis of TiO_2 QDs due to the shorter reaction time, rapid transfer of heat and energy, understood as an ecological process, which requires less energy consumption than conventional heating processes and increased product yield[57,63-66].

Microwave-assisted heat treatment provides a more efficient way of heating compared to conventional hydrothermal synthesis, as heat is immediately directed to the solution whereas, in a conventional oven, the heat needs to dissipate from the oven to the reactor and then to the real solution. It is, therefore, a faster method that usually takes a few minutes, compared to hydrothermal, which can last up to several hours[66,67].

Microwave reactors operate at the frequency of 2.45 GHz, corresponding to a pulse energy of 0.0016 eV, being a very weak energy to break chemical bonds, consequently, microwaves are not able to induce chemical reactions, but they offer a

very efficient heating tool. Irradiation of a reaction mixture at the microwave frequency results in the alignment of dipoles or ions in the electric field. Due to the fact that the applied field oscillates, the dipole or ionic field has to continuously realign itself, which produces energy in the form of heat through molecular friction and dielectric loss[68-70].

Microwave-assisted hydrothermal synthesis begins with the rapid and homogeneous heating process, the heat transmitted directly to the material (if it absorbs microwaves) or to the solvent (H_2O) through molecular interactions with the electromagnetic field, generating molecular vibrations, as shown in Figure 9. The efficiency with which electromagnetic radiation is converted into heat is dependent on the solvent dielectric properties[71,72].

Figure 9 Water molecules in an alternating electric field under microwave irradiation
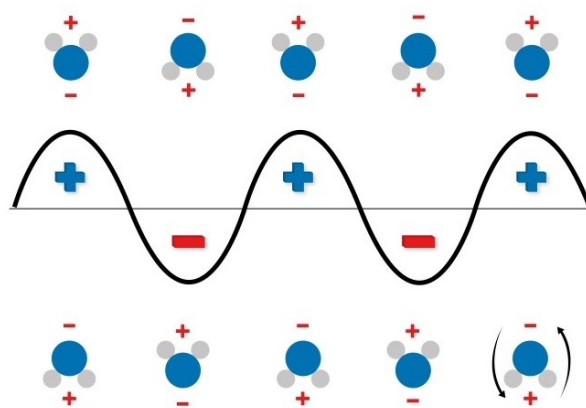
Source: Zhu and Chen (2014)[72]

The technique choice for this work was based on previous research from the group, which had already started synthesis studies using microwave methodology and presented excellent results.

Chapter 3 - Highly Enhanced Adsorption and Photocatalytic Performance of TiO₂ Quantum Dots Synthesized by Microwaves for Degradation of Reactive Red Azo Dye[1]

3.1 Introduction

In the last decades, the study of semiconductor low-dimensional structures has opened a vast field of study for scientists as a result the characteristic size of the blocks that characterize the microstructure (crystallite size) decreases to dimensions comparable to the critical lengths of some physics phenomena, changing properties which depends, mainly, of the size and chemical composition of its atomic structure, like sorption, catalytic, magnetic, optical and thermal. Among the low dimensional structures, the quantum dots (QDs) demonstrate extraordinary properties due to the confinement of particles in all three dimensions[32,34,38,73].

In this regard, nanostructured materials are structurally composed of two components: one crystalline, with dimensions on the order of some nanometers that preserves the structure of a bulk crystal, and another called interfacial component, which comprises several types of defects, grain boundaries, interphase boundaries, dislocations, etc. The volume fraction of the two components is comparable, the high density of interfaces and the high number of atoms present in the interfacial component[39,40] allows the manipulation, for example, introducing new surface modification or via thermic treatment[74-76] leading to the possibility of tuning the physical properties for specific technology, like high-efficiency solar cells[77] photocatalytic activity[78], self-cleaning surface[79], energy storage systems[81] and sintering[30].

Recently, the improvement of photo conversion efficiency (PCE) per unit area and reduction of the value per watt in quantum-dot-sensitized solar cells (QDSSCs) have received attention together of the foremost promising configurations within the third-generation electrical phenomenon devices[30,31]. Many researchers have been studying manners to increase the PCE of QDSSCs by the optimization of photoanode structure combining different morphologies of TiO₂[83-85] thanks to QDs distinctive optoelectronic properties, including bandgap modulation by size control, high molar extinction coefficients, large intrinsic dipole moments, multiple exciton generation, and simple fabrication methods[86-89].

Considering the properties mentioned investigations are made in application of similar processes, such as artificial photosynthesis[60,90] and heterogeneous photocatalysis[27,78,91]. The first step of both processes involves the adsorption of molecules on the surface of the catalyst, which is directly related to the productivity of the process[92]. Therefore, materials with a high specific surface area (SSA) and low energy barrier to adsorption can have their performance improved by manipulating the catalyst surface. Da Silva et al.[60] present a detailed study on CO_2 and H_2O adsorption on undoped and alkaline earth metals doped TiO_2 nanoparticles, the study shows TiO_2 modified adsorbs more CO_2 than pristine TiO_2 mainly due to the increase in SSA. Liu et al.[91] proposed a new strategy to degradation of oil pollutants for water remediation. Generally, the good photocatalytic activity is ascribed to the inherent oxygen vacancies, which provide an internal Z-scheme of the electron transition (typically constructed by a heterojunction that consists of two composites). The main purpose of the research is that besides the heterojunction structures, highly proficient photocatalysts could also be designed by a new approach that introduces deep energy levels in the band gap of low dimensional materials, like the incorporation of vacancies and conjugation of other elements.

To processing these classes of materials, more precisely TiO_2 QDs, some routes have been explored. The microwave synthesis is an environmentally friendly method that offers high homogeneity and yield in short synthesis times[72]. A few studies address the production of QDs in a microwave reactor, but they do not consider pressure and temperature control, using rather a conventional microwave equipment[93,94]. Alternatively, sol-gel[79,95] or hydrothermal methods[2] at higher temperatures might be used, but with lower heat homogeneity in reactions. Therefore, microwave synthesis produces small and homogeneous nanoparticles, explained by the high reaction rate and volumetric heating[68,96].

In this context, the present work is based on the manipulation of interfacial component of QDs by the adjustment (time and temperature) of parameters of microwave synthesis of TiO_2 QDs in order to optimize their photocatalysis efficiency. The adsorption process and degradation of reactive red azo dyes was evaluated. Structural and morphological properties, as well as recycling features, are also measured.

3.2 Experimental

3.2.1 Raw Materials and Microwave Synthesis

TiO_2 QD's were synthesized by the microwave-assisted hydrothermal method. The experimental procedure was previously reported by Falk et al. (2018)[97]. The synthesis started with the hydrolysis of titanium tetraisopropoxide (TTIP97%, Sigma-Aldrich) in an aqueous solution (18.2 MΩ cm^{-1}, ultra-pure Milli-Q) and nitric acid (HNO_3, 65 %, Vetec), under continuous stirring at 600 rpm, with H_2O: Ti^{4+} =110:1 and H^+: Ti^{4+} = 0.35 molar ratios at room temperature.

Stirring continued for further 30 min under the same conditions. Then 30 mL from the solution was transferred to a borosilicate glass sealed vessel, which was placed in a commercial microwave digestion system (Monowave 300, Anton Paar). The system operated at a frequency of 2.45 GHz with a maximum power of 850 W, which was modulated from 0 to 100% during the reaction. Initially, time trials (10, 20, 30, and 60 min) were performed at 180 °C. After defining the optimized time as 10 min, the study of temperature (120, 140, 160, and 180 ºC) was accomplished.

Finally, the samples were centrifuged at 4000 rpm for 10 min using a multi-purpose benchtop equipment and washed 3 times with deionized water. TiO_2 QD's were dried in an oven at 100 ºC for 48 h.

3.2.2 Quantum Dots Characterization

The crystalline phases of nanoparticles were evaluated by X-ray diffraction (XRD, PW-1830 X'Pert, Philips) using Cu-$k\alpha$ radiation at 40 kV and 40 mA. Data were collected in the 2θ range of 20-80º. The average crystallite size was calculated using the Scherrer equation[98] by the most intense peak located at about 2θ ~ 25.3º of XRD patterns. To study the influence of the interfacial component (all types of defects) on the properties of TiO_2 QDs, the volume fraction of this component was estimated. The interfacial component produces a diffuse scattering signal and not is possible to separate its contribution from the XRD background. The evaluation of the background contribution to the XRD pattern and its subtraction yields the contribution of the TiO_2 QDs. For the background subtraction Origin software was used. The ratio between the integrated intensity from the TiO_2 QDs and the integrated total intensity XRD pattern yields the crystalline volume fraction and the balance is the interfacial component.

Raman spectroscopy (Renishaw-2000) was performed with a coupled microscope (Leica DM LM, argon laser of 514.5 nm).

Transmission electron microscopy (TEM, JEOL, JEM 2100F, 100 kV) was used to verify the QDs size and morphology. The samples were dispersed in isopropyl alcohol for 10 min in an ultrasonic bath. One single drop of the suspension was placed on a carbon-coated copper grid, which was dried for 12 h at room temperature.

The specific surface area (SSA) was measured according to the multi-point BET method (Monosorb Surface Area Analyzer, Nova 1200e, Quantachrome) after degassing the samples at 180 ºC for 2 h.

3.2.3 Adsorption and Photocatalysis

The adsorption and photocatalysis study were held in a batch reactor to compare TiO_2 QDs synthesized at different temperatures. An aqueous solution (0.5 L) of 20 $mg \cdot L^{-1}$ dyes (Reactive Red, RR141, or Methyl Orange, MO) was used at pH ~6. TiO_2 nanoparticles (0.25 $g \cdot L^{-1}$) were added to form a suspension, which was magnetically stirred for 2 h at 400 rpm and room temperature.

To measure the photocatalytic activity, a UV-B light source (5 W) was immersed inside the reactor. The analyses were carried out either without adsorption or with 15 min adsorption. The concentration of the dye adsorbed on the catalytic surface was calculated by the difference between the initial dye concentration and that remaining in the solution after the equilibrium. The solutions were magnetically stirred for 30 min at 400 rpm and room temperature.

The QDs reuse was tested in 3 cycles for both processes – adsorption and photocatalysis. At the end of each cycle, 20 ppm dye was fed in the reactor. The dye removal from the solution was detected by the respective major absorbance peaks (544 nm for RR141, and 465 nm for MO) using UV-vis spectrophotometry (SpectraMax Plus 384, Molecular Devices).

3.3 Results and Discussion

3.3.1 Microwave Synthesis and Quantum Dots Characterization

TEM and XRD analyses of TiO_2 samples – synthesized between 10 and 60 min of microwave irradiation – did not show significant differences. In this regard, the 10-min treatment was selected since it represents higher energy savings for the process.

Figure 10 shows TEM images of the samples synthesized by microwave hydrothermal treatment at different temperatures. The small agglomerates observed are due to drying, because of the hydrophilic and highly energetic surface of the nanoparticles. Spherical shaped nanoparticles with an average size of ~5 nm (measured with the aid of ImageJ software) are observed. Thus, microwave-assisted synthesis led to highly homogeneous crystalline nanoparticles using low temperatures (120 °C) at significantly shorter times than traditional processes[99-101].

Figure 10 - TEM micrographs of TiO$_2$ QDs synthesized at different microwave temperatures: (a) 120 °C, (b) 140 °C, (c) 160 °C and (d) 180 °C.
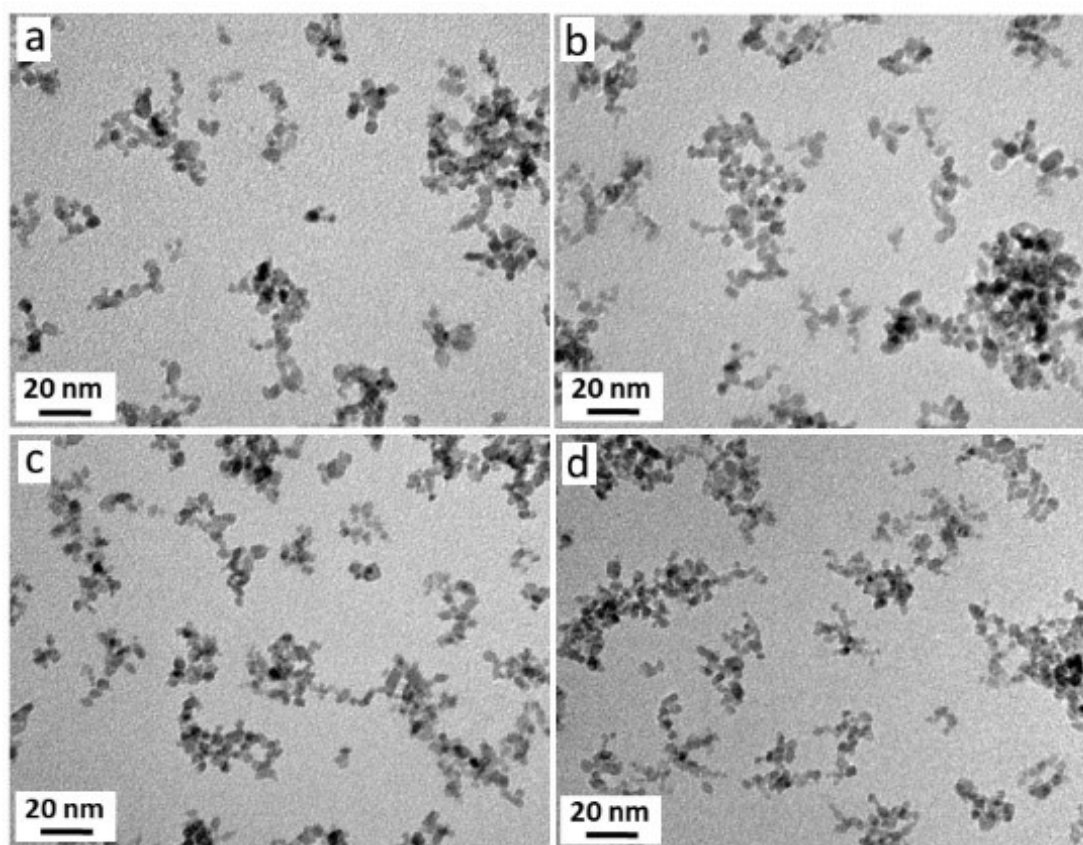
XRD patterns spectra of the TiO$_2$ QDs synthesized by microwave hydrothermal treatment for 10 min at different temperatures (120, 140, 160, and 180 °C) are presented in Figure 11(a), respectively. The peaks at 2θ values of 25.3°, 37.8°, 48.0°, 55.1°, and 62.7° can be indexed to (101), (200), (211) and (204) crystal planes of crystalline phase anatase (JCPDS No. 01-071-1166). Thus, the anatase phase is prevalent at all samples with a small formation of brookite, corresponding to the peak at 31° (JCPDS No. 01-

076-1936). As a complement, the respective Raman spectra (Figure 11(b)) show the bands centered at 152, 402, 520, and 645 cm^{-1}. According to the literature[97,102], the bands at 150, 195, 398, 517 and 640 cm^{-1} are assigned to the modes $E_{g(1)} + E_{g(2)}$, B_{1g}, $A_{1g} + B_{1g(2)}$ and $E_{g(3)}$ of the anatase phase, respectively. Hence, the XRD and Raman spectra show accordance in all cases.

Figure 11 (a) XRD patterns of TiO$_2$ QDs synthesized by microwave hydrothermal treatment at 120, 140, 160, 180ºC and (A-TiO$_2$) the phase anatase corresponding to (JCPDS No. 01-071-1166), the (*) corresponding a small formation of brookite (b) Raman spectra of TiO$_2$ QDs
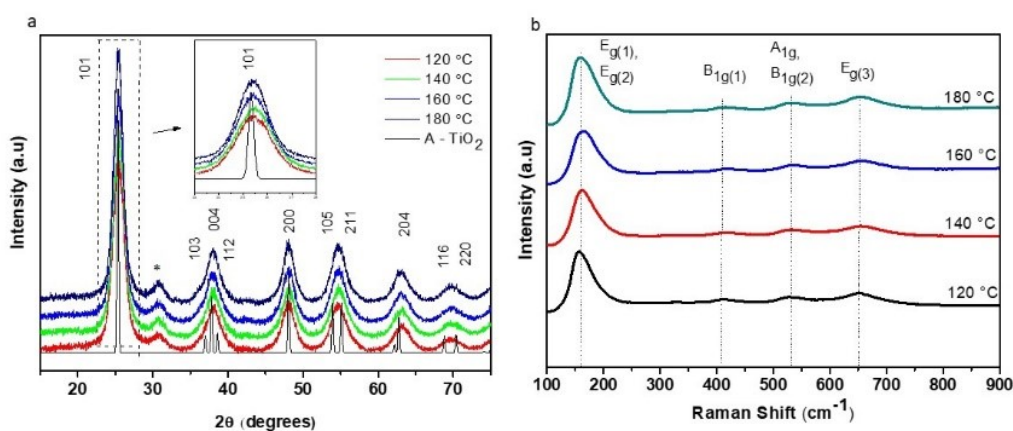
The full width at half maximum (FWHM) of XRD, the crystallite sizes calculated by the Scherrer equation, the crystalline/interfacial component fractions, and the specific surface area of the QDs are shown in Table 1. With the increase of the synthesis temperature, there is a decrease in the amount of interfacial component (Figure 12). There is also an increase in the average crystallite size of the samples, following the decrease in the amount of interfacial component. The results of specific surface areas do not show significant trends.

Therefore, low-temperature microwave synthesis produced powders with a small average crystallite size, associated with a larger amount of interfacial component. A thermodynamic/kinetic approach can clarify this behavior. Higher synthesis temperatures lead to higher internal pressure in the reactor, producing a more favorable environment to enhance the crystallinity, decreasing the interfacial component of the QDs[69]. The high temperature favors atomic mobility, while the high pressure facilitates the structural order. However, in the synthesized powders, the amount of interfacial component obtained favors the storage of internal energy at low temperatures. To

confirm the effect of high temperature on the structural characteristics of QDs, thermal treatment at 650 ºC was performed on the sample synthesized at 120 ºC. By the analysis of the XRD pattern, the material became highly crystalline with the nucleation of the rutile phase. Also, the interfacial component was strongly reduced (~ 5%).

Table 1 The full width at half maximum (FWHM) of XRD, average crystallite size, crystalline/interfacial component and specific surface area of TiO$_2$ QDs

TiO$_2$ Samples	Microwave temperature (ºC)	FWHM	Apparent Crystallite Size (nm)	Crystalline/interfacial component (%)	Specific Surface Area (m^2·g^{-1})
Quantum Dots	120	1.81037	5.0	40/60	292
	140	1.78464	5.1	44/56	257
	160	1.65614	5.5	45/55	253
	180	1.48582	6.2	48/52	245

Figure 12 - TiO$_2$ average crystallite size and interfacial component percentage as a function of QDs synthesis temperature
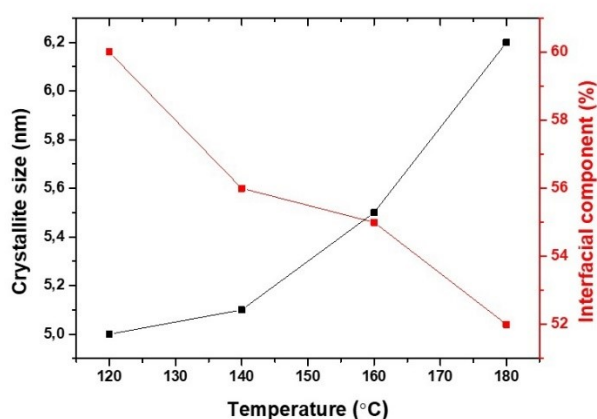
3.3.2 Adsorption

It is well established that adsorption plays an important role in heterogeneous photocatalysis[92]. It can be defined either by the kind of interaction – chemisorption

and/or physisorption – or by the irregularities found in the surface. The adsorption precedes the chemical reaction on the catalyst surface. When the chemisorption takes place, the reactant molecules interact with the catalyst surface. If active sites are available – depending on the number of surface defects – they define how energetic the nanoparticle surface will be[69,103].

Figure 4a shows Reactive Red (RR141) adsorption with nanoparticles synthesized at different temperatures. For the synthesized particles, the adsorption rate is higher in the first 5 min in all cases. The higher the QDs synthesis temperature, the lower the adsorption performance. In the sample synthesized at 120 ºC, 65% RR was adsorbed in the first 5 min comparing to the 180 ºC sample, which reached just 29%. In this case, two factors may explain adsorption behavior: the reactivity of RR and the higher interfacial component percentage present in QDs (Table 1).

RR is a diazo dye ($R_2C = N_2$), which contains the reactive monochlorotriazine system. It is a large molecule (Figure 13a) with eight sulfonic groups ($-SO_3^-$) corroborating the highest adsorption. On the other hand, only 26% and 0.1% of Methyl Orange (MO), which has a single negative charge (Figure 13b), was adsorbed by the QDs synthesized at 120 and 180 ºC respectively. Therefore, the more negative charges available, the higher the ionic force, and the higher attraction by the positive surface of the adsorbent.

Concerning the influence of the amount of interfacial component, the results in Figure 4 confirm the hypothesis described before. The QDs synthesized at a lower temperature (120 °C) show the best adsorption performance since they present a greater fraction of the interfacial component in its composition, which retains a higher amount of stored internal energy and, therefore, higher Gibbs free energy[81,92]. This high surface energy produces the greatest thermodynamic driving force that accelerates the adsorption kinetics.

Figure 13 Adsorption of azo dyes with TiO_2 QDs: (a) Reactive Red (RR141); (b) Methyl Orange (MO); and their respective molecular structures
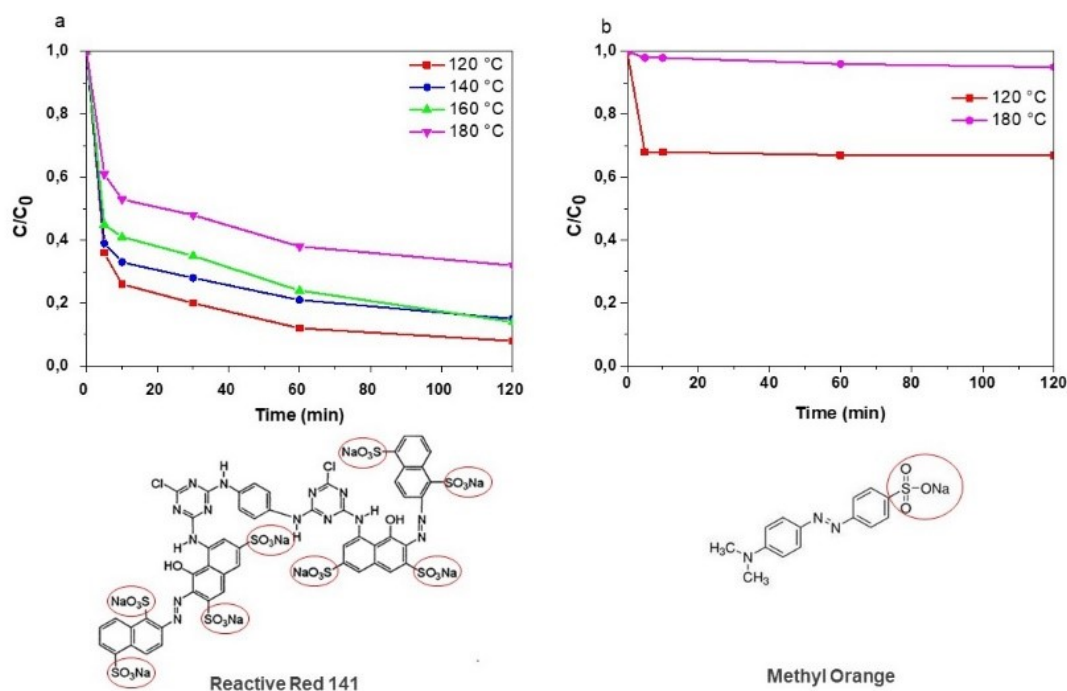
Thus, it was found that the surface of QDs is very reactive and that the adsorption took a long time to reach equilibrium. In this case, 15 min were defined for the adsorption process to take place, because in ~10 min the maximum amount of dye is adsorbed onto the catalytic surface.

3.3.3 Photocatalysis

The photocatalytic performance of QDs synthesized at different temperatures were available. Figures 14a and 14b compare the photocatalysis with and without previous adsorption, respectively. When the UV-B lamp is turned on from the beginning of the process (Figure 14b), all samples presented a similar behavior taking 15 min of irradiation to degrade 100% RR141 dye. With a previous adsorption process (Figure 14a), in only 5 min 100% RR141 dye was degraded by the QDs synthesized at 120 ºC. This can be explained by the first reaction occurring on the catalyst surface. Since the QDs synthesized at lower temperature have a higher interfacial component than the other samples, they adsorb a larger amount of dye in the first minutes; when the lamp is turned on, this amount of adsorbed dye is rapidly degraded.

Figure 14 Photocatalytic degradation of RR141 dye by TiO_2 quantum dots: (a) with adsorption (b) without adsorption
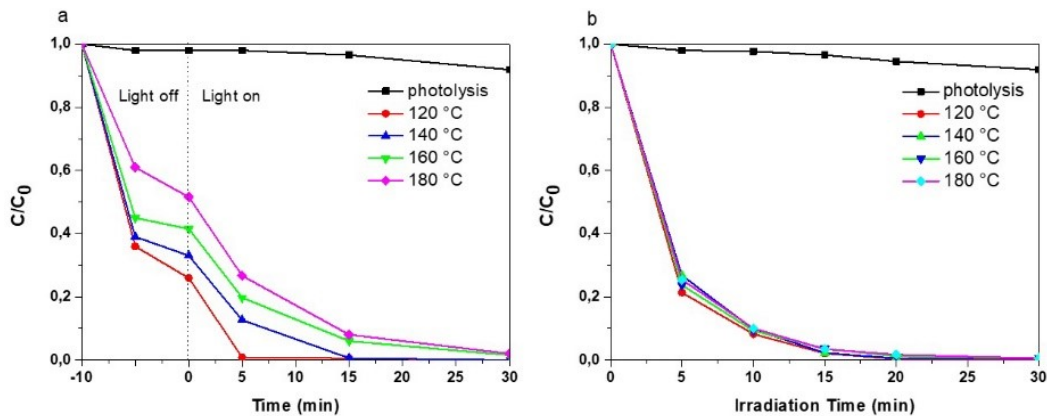
Rajabi[104] described a possible mechanism for the photocatalytic activity of QDs photocatalysis comprising: (i) diffusion of reactants to the surface of photocatalyst particles; (ii) adsorption of reactants onto the surface; (iii) reaction on the surface. This mechanism may explain the photodegradation efficiency when comparing QDs with different percentages of the interfacial component since the adsorbed dye will be degraded sooner than the dye in the solution.

The reuse of photocatalysts is necessary to reduce processing costs. Thus, the QDs synthesized at 120 ºC, which presented the best performance in adsorption/photocatalysis were reused in 3 cycles, as shown in Figure 15, for the degradation of RR dye. The adsorption process decreases its efficiency after each cycle, probably due to a more saturated surface. Hence, the photocatalysis takes a longer time to degrade the RR dye in a new cycle.

Figure 15 - Photocatalytic degradation of RR141 dye by TiO_2 quantum dots synthesized at 120ºC and recycled
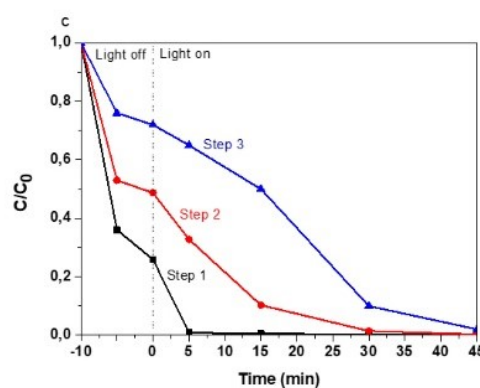
3.4 Conclusions

TiO$_2$ QDs with an average size of 5 nm and a specific surface area of ~292 m^2·g^{-1} were synthesized by microwave hydrothermal treatment. Highly homogeneous QDs were obtained at a lower temperature (120 °C) and a shorter time (10 min) than those in traditional processes. XRD patterns showed anatase as a major crystalline phase and an increase in the interfacial component as the microwave temperature decreases, resulting in a highly energetic surface and super adsorbent QDs. The higher the adsorption process, the faster the photocatalysis process. Finally, the synthesized TiO$_2$ QDs presented a high absorption and photocatalytic activity, just by changing the temperature parameters of the microwave. In the best case, 100% of RR141 dye was degraded in ~5 min. As well defined the parameters of the synthesis, the prospects are the properties manipulation of the TiO$_2$ QDs by doping, as well as the improvement of thermodynamics characterization techniques on the surface of QDs.

Chapter 4 - Ca²⁺/La³⁺ doped TiO₂ quantum dots highly adsorbent synthesized via hydrothermal microwave-assisted treatment for Tetracycline degradation using visible light[2]

4.1 Introduction

Many variables can affect the efficiency of a photocatalyst such as a particle/grain size, specific surface area, crystalline and interfacial component, light intensity, catalyst concentration, and adsorption capacity[105-107]. To understand the influence of these variables on catalysis, investigations on nanostructured materials have increasingly grown.

The reduction in particle and/or grain size is followed by an increase in surface area and an enrichment of interfacial component, which comprises several types of surface defects (grain boundaries, interphase boundaries, dislocations, vacancies, edges, corners, and faces of the crystal) in nanoparticles when compared to their bulk counterparts[40]. Commonly, the volume fraction of the two components is comparable, leading a strong dependence of the material properties on the atomic arrangements of the interfacial phase[39]. Manipulation of these atomic arrangements leads to the possibility to design new materials with unprecedented properties for specific technological applications[108].

Among nanoscale materials, quantum dots (QDs) are tridimensional structures with dimensions between 2 and 10 nm, defined as particles smaller than the exciton Bohr radius, where the critical length of physical phenomena is comparable. When the layers thickness of a superlattice is comparable with the electrons wavelenght at the Fermi edge, discrete energy levels for electrons and holes in the quantum wells will be formed[19,109-111]. Such confinement effects result in different mechanical, transport and optical properties. The higher surface area to volume ratio of QDs make them excellent nano photocatalysts, particularly for environmental applications, such as water and air purification[37,112].

TiO₂ nanoparticles are widely used and investigated as semiconductors due to their excellent chemical stability, low cost, and easy production. However, the electronic properties need to be improved so that the energy needed to excite the electrons from the

---

[2]Submitted for publication.

valence band to the conduction band is smaller than the bulk TiO_2 gap, known to be ~ 3.2 eV for anatase crystalline phase[49]. This reduction would make it possible to use visible light for photodegradation reactions more efficiently, since solar radiation in the ultraviolet (UV) region represents only 5% of the power of solar energy that reaches the earth, while 43% of the solar radiation correspond to visible region[113].

Introduction of doping ions is the most plausible alternative to shift the absorption band to a longer wavelength, resulting in visible light absorption[114-116]. The effect of metallic ionic dopants on photocatalytic activity is complex. The change induced in the photocatalytic activity results from a sum of modifications, including the light absorption capacity of the TiO_2 photocatalyst; adsorption capacity of substrate molecules on the catalyst surface; and the interfacial charge transfer rate[54]. As the dopant concentration increases, the space charge region becomes smaller, and the depth of light penetration into the TiO_2 nanoparticles exceeds the space charge layer. Recombination of photogenerated e^-/h^+ pairs in the semiconductor increases because there is no driving force to separate them[53]. Consequently, there is an optimal concentration of doping ions to make the thickness of the space charge layer substantially equal to the depth of light penetration.

Doping can be performed with different ions and can take place in a substitutional or interstitial manner[117,119]. The mechanism will depend on the ionic radius, the valence of ions of the dopant, or its solubility in the host's crystal lattice. When the dopant is a little immiscible in the lattice of the crystallites, it frequently segregates to the grain boundary. If many atoms segregate to the grain boundary the free energy of the system is severely reduced, increasing the nanostability of the system, preventing grain growth, and can add intermediate electronic states facilitating charge transport[14,40,59,58]. A thermodynamic approach to explain this mechanism is following in equation (9).

$$\sigma_i = \sigma_0 - \Gamma_i \Delta H_{seg} \qquad (9)$$

Where σ_i is the interfacial energy, σ_0 is the interfacial energy of the undoped material; Γ_i is the solute excess at the interface; and ΔH_{seg} is the enthalpy of segregation. The interface term is described as solid-vapor and solid-solid contributions. The solid-vapor interface is often referred to as the surface, and the solid-solid interface is commonly referred to as grain boundary.

In case of excess dopant, it can remain on the semiconductor surface and also change the adsorption patterns, as reported by da Silva et al. (2020)[60] in TiO_2 doped with alkaline-earth ions. Following this line, Rafieh et al. (2021)[61] synthesized pure and Ca and La doped TiO_2 nanoparticles via sol gel method in order to increase the adsorption capacity of the N719 dye for application on dye-sensitized solar cell (DSSC) anode. As a result, they got TiO_2 has particle size of 76.7 nm, Ca doped and La doped TiO_2 with 61.1 nm and 51.0 nm, respectively. With the reduction in particle size, surface area increases to doped Ca (98.1 $m^2.g^{-1}$) and La (117.6 $m^2.g^{-1}$) while pure TiO_2 is 78.3 $m^2.g^{-1}$. They showed that doping prevents nucleation and growth of particles during synthesis and calcination at high temperature. Additionally, doping resulted in decreasing the band gap. Pure and Ca doped TiO_2 exhibited good correlation to both of the isotherms Langmuir and Freundlich adsorption.

Herein, we report a facile and safe method to prepare and reproduce the anatase pure and Ca^{2+}/La^{3+} doped TiO_2 QDs with a high specific surface area and a highly adsorptive. The prepared QDs had a high visible light absorption and exhibited excellent activity for visible light photocatalytic.

4.2 Experimental

4.2.1 Raw Materials and Microwave Synthesis

The doping of QDs occurred by modification of the synthesis described in Frizzo (2021)[120]. First, 0.5, 1.0, 3.0 and 5.0 mol% of the Ca^{2+} ion and 1.0, 2.0, 3.0 and 4.0 mol% of the La^{3+} ion replaced Ti^{4+}. Calcium nitrate tetrahydrate P.A ($Ca(NO_3)_2.4H_2O$, Neon) and lanthanum(III) nitrate hydrate ($La(NO_3)_2.H_2O$ 99.9%, Sigma-Aldrich) were added to the acidic aqueous solution for 10 minutes (18.2 $M\Omega\ cm^{-1}$, ultra-pure Milli-Q) (HNO_3, 65 %, Vetec), previously to the titanium tetraisopropoxide precursor (TTIP97%, Sigma-Aldrich) under continuous stirring at 600 rpm for further 30 min. After hydrolysis of the titanium tetraisopropoxide, the reaction was transferred to a borosilicate glass sealed vessel containing, which was placed in a commercial microwave digestion system (Monowave 300, Anton Paar). The heating ramp was adjusted to 5 min, and the reaction time was 10 min at 120 °C. The cooling temperature was set to 55 °C. After microwave treatment the samples were centrifuged at 4500 rpm for 30 min using a multi-purpose benchtop equipment (Kasvi, K140815C) and washed 3

times with ethanol. TiO_2 QD's were dried at 100ºC for 48h and macerated for characterization.

4.2.2   Quantum Dots Characterization

The crystalline phases of nanoparticles were evaluated by Benchtop X-ray diffractometer with advanced detector (XRD, Rigaku MiniFlex 600) operating at 15 mA and 40 kV. The diffraction patterns were recorded in the 2θ range of 20-80º. The average crystallite size was calculated using the Scherrer equation[144] by the most intense peak located at about 2θ ~ 25.3º of XRD patterns. The interfacial component produces a diffuse scattering signal, and it is not possible to separate its contribution from the XRD background. Thus, the fraction volume of the interfacial component was estimated evaluation of the background contribution to the XRD pattern. The ratio between the integrated intensity from the TiO_2 QDs and the integrated total intensity XRD pattern yields the crystalline volume fraction and the balance is the interfacial component[45,120]. Raman spectroscopy analyses were performed using Anton Paar Cora 5200 instrument equipped with a laser source of 785 nm. Data were collected in the range of 100-800 cm^{-1}.

The specific surface area (SSA) was measured according to the multi-point BET method (Monosorb Surface Area Analyzer, Nova 1200e, Quantachrome) after degassing the samples at 100 ºC for 1 h.

The UV–Vis absorbance spectra of QDs dispersed in ethanol were collected with an Ocean Optics USB4000 spectrophotometer. The zeta potential measurements were performed at 25 °C in aqueous solution using a Zetasizer Nano ZS from Malvern. The experimental procedure for evaluating the adsorption and catalytic activity involved a black box containing a magnetic stirrer, and a round glass vessel. The adsorption and catalytic activity test were performed in a 250 mL aqueous solution tetracycline at 13 ppm. TiO_2 QDs 0.125 g were added to form a suspension, which was magnetically stirred at 400 rpm at room temperature. The adsorption process was carried out in the dark for 15 min. The antibiotic concentration adsorbed on the catalytic surface was calculated by the difference between the initial and final antibiotic concentration in the solution. To measure the photocatalytic activity a visible radiation source low-pressure mercury vapor lamp (105 W, 400–750 nm) was turned on. At each time interval, an aliquot was removed and centrifuged at 4500 rpm. The supernatant was collected, and

the antibiotic degradation reading (λmax = 357 nm) was performed in the UV-vis spectrophotometer (SpectraMax Plus 384, Molecular Devices).

4.3 Results and Discussion

4.3.1 Quantum Dots structural and electronical characterization

Figures 16 and 17 show XRD patterns and Raman spectra of pure (0%) and doped TiO_2 QDs with range 0-5 mol% of Ca^{2+} and La^{3+} ions synthesized and thermally treated at 120 ºC via microwave, respectively. Figures 16(a) and 17(a), present in both patterns anatase as the major crystalline structure, detailed in Frizzo et al., (2021)[120]. This indicated that the doping process kept anatase as main crystalline phase. The crystallite sizes in Table 2 were estimated by Scherrer[144] equation using the half-maximum full width (FWHM) of the most intense peak of the anatase crystalline phase (101) of XRD pattern. For all samples, doped and undoped, the crystallites sizes were between 4.9-5.0 nm, there was no considerable variation.

In Table 1 an increase of the interfacial component fraction and consequent decrease of the crystalline phase were observed. Such modifications are due to defects introduced in the system by dopants ions as lattice dislocations, vacancies and grain boundaries, which can elucidate the differences among the values of specific surface areas to the same crystallite size.

The ionic radius of the Ca^{2+} (0.100 nm) and La^{3+} (0.103 nm) are significantly bigger than Ti^{4+} (0.061nm)[61]. Adding up their different valences with low solubility in the crystalline lattice these doping ions are often segregated to the grain boundaries. In this way, grain boundary free energy can be reduced. This clarifies why excess dopant decreases specific surface area. For example, for TiO_2 QDs with 1 mol% dopants of Ca^{2+} and La^{3+}, both samples had a larger surface area than for pure QDs. This means that in this proportion of doping ions they preferentially occupy the grain boundary regions (solid-solid)[121]. On the other hand, for samples with a higher % of dopant, the excess of dopant migrates to the interface (solid-vapor). For the sintering process, this is positive because it prevents nucleation and grain growth during the calcination at high temperature [14,39,81,122].

The biggest difference between the specific surface area of the samples with 1 mol% of Ca^{2+} (412.1 $m^2.g^{-1}$) and 1 mol% of La^{3+} (309.51 $m^2.g^{-1}$) can be attributed to Ti-O-Ca and Ti-O-La interactions in the boundary regions of the atomic structure. Ions

Ca^{2+} and La^{3+} have more affinity with oxygen atoms than those of Ti^{4+}, which can reduce Ti^{4+} ions to Ti^{3+}. Thus, the electronic density of the dopants will reduce, consequently, for each dopant the chemical bond length will not be the same, and there will be different imbalances in the charge surface of the TiO_2 lattice[61,123-125].

The charges compensation mechanism induces the formation of oxygen and titanium vacancies and it can be observed by Raman spectra in Figures 16 and 17. As Raman signal of TiO_2 is sensitive to the vibrational mode of oxygen ions in the Ti-O bond, the strongest signal of anatase corresponds to $E_{g(1)}$ mode, originated from O-Ti-O bond bending vibration[126]. This main $E_{g(1)}$ mode shifted toward a lower vibrational frequencies (redshift). Redshift means that frequency of phonons interacting with the incident photon decreased, that is the photon absorbed by the material created an e^-/h^+ pair that suffered scattering with phonons or with perturbations in the crystal lattice until recombined and emitted a photon with different energy[127]. Moreover, if a crystal is subjected to tensile stress or as the chemical bond length increases and the force constant remains the same, the vibrational frequency decreases and a shift red is observed[128,129]. In addition, broadening in the full width at half maximum (FWHM) of the $E_{g(1)}$ peak in Table 2 of the sample with 1 mol% of Ca^{2+} (49.39) is bigger than 1 mol% of La^{3+} (46.57) comparing to pure TiO_2 QDs (43.51). It has been widely understood that shifts in the $E_{g(1)}$ peak position and peak broadening are resulting from the oxygen non-stoichiometry and account for the narrow bandgap by shallow trap levels for electrons[130-135].

Figure 16 - (a)XRD patterns, (b)Raman spectra of pure (0%) and doped TiO2 QDs with 1, 3, and 5 mol% of Ca^{2+}, synthesized by microwave hydrothermal treatment at 120 ºC
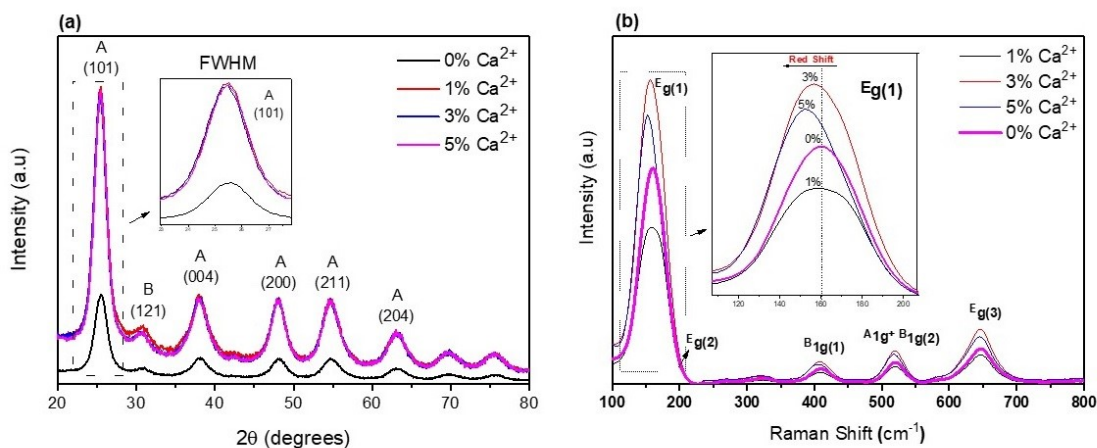
Figure 17 - (a)XRD patterns, (b)Raman spectra of pure (0%) and doped TiO$_2$ QDs with 1, 2, 3 and 4 mol% of La^{3+} synthesized by microwave hydrothermal treatment at 120 ºC
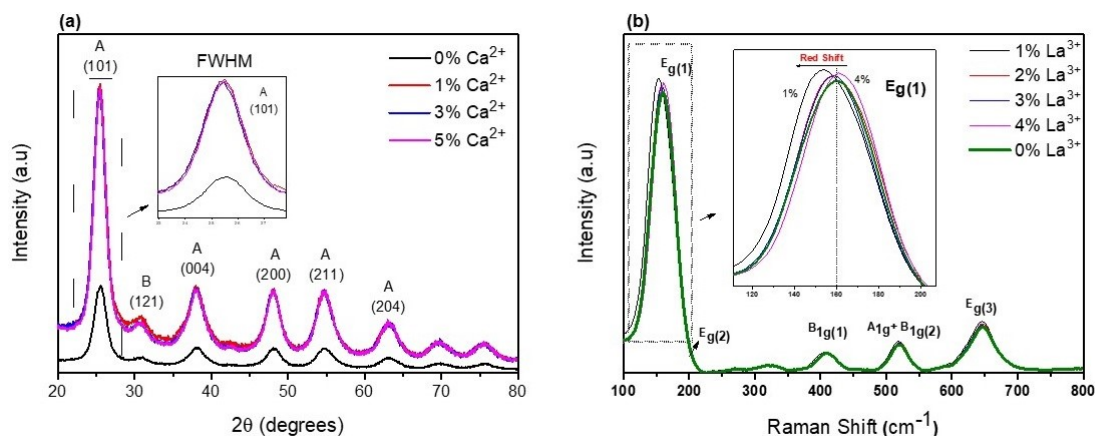
Table 2 - The full width at half maximum (FWHM) of XRD and Raman, average crystallite size, crystalline/interfacial component, specific surface area and of TiO$_2$ QDs

TiO$_2$ QDs mol% doping	FWHM XRD (101)	Apparent Crystallite Size (nm)	Interfacial component (%)	Specific Surface Area (m$^2 \cdot$g^{-1})	FWHM Raman E$_{g(1)}$ mode (cm^{-1})
0%	1.85201	4.9	60	292.81	43.51
1% Ca^{2+}	1.80979	5.0	64	412.19	49.39
3% Ca^{2+}	1.84749	4.9	62	281.50	45.76
5% Ca^{2+}	1.83022	4.9	62.5	283.04	45.30
1% La^{3+}	1.82324	5.0	64	309.51	46.57
2% La^{3+}	1.82775	4.9	63.5	287.41	44.33
3% La^{3+}	1.83034	4.9	62.5	276.76	42.73
4% La^{3+}	1.84165	4.9	63	283.10	41.75

4.3.2. Adsorption and Photocatalysis

Figure 18 presents the results of adsorption of the pure and Ca^{2+}/La^{3+} doped TiO$_2$ QDs. Due high specific surface area and interfacial component, the QDs have a superabsorbent surface. Thus, the adsorption took a long time to reach equilibrium. Therefore, 15 min were defined for the adsorption process to take place, because it is when the maximum amount of tetracycline is adsorbed onto the catalytic surface.

The high amount of tetracycline adsorbed onto surface of QDs can also be related to zeta potential measurements at pH 3.6, presented in Table 3. The values of zeta potential indicate a QDs surface positively charged, which suggests a good interaction with tetracycline anionic groups, as evidenced by the high adsorption rates shown in Figure 18. Zeta potential of an electrostatically stabilized colloidal suspension should be at least ±30 mV. The higher value, more stable in the suspension, as the loaded surfaces repel each other and reduce the natural tendency to agglomeration. Both samples present suitable zeta potential values, which indicated good colloidal stability of the QDs. All samples demonstrate good long-term stability, and the aqueous colloidal suspensions are stable for more than 2 months without any noticeable sedimentation. The sample with 1 mol% Ca^{2+} presents a higher adsorption rate because it has a greater specific surface area comparing to the other samples, that show a similar adsorption rate as they have a close specific surface area.

Figure 18 - Adsorption of the tetracycline antibiotic on pure and Ca^{2+}/La^{3+} doped TiO_2 QDs
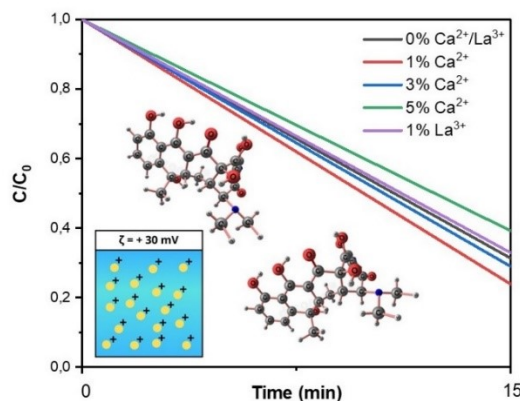
Direct optical band-gap values, shown in Figure 20(b) and Table 3, were determined using the Tauc method based on the following equation (10):

$$\alpha h\nu = A(h\nu - Eg)^{n/2} \quad (10)$$

Where n refers to the nature of the transition, here we use $(n = 2)$[39]. By plotting $(\alpha h\nu)^2$, vs energy of absorbed wavelength and extrapolating the linear region of lowest energy of the graph it was found that pure TiO_2 QDs have a band gap of 3.03 eV, which is lower than the previously reported value of 3.2 eV for the anatase phase[140] and its due to the low crystallinity are of the material. La^{3+} doping led to an increase in E_{bg} while the samples containing Ca^{2+} achieved the lowest E_{bg} overall at 2.72 eV, making them excitable with the lower energy radiation of the visible spectrum.

Table 3 Zeta potential (pH 3.6) and band gap of the pure and Ca^{2+}/La^{3+} doped TiO_2 QDs

TiO₂ QDs mol% dopant	Zeta potential (mV)	Band Gap (eV)
0%	+30.7	3.03
1% Ca²⁺	+26.8	2.72
5% Ca²⁺	+28.1	2.80
1% La³⁺	+30.0	3.14
4% La³⁺	+28.0	3.04

By the e^+/h^- pair confinement in three dimensions[34,109], QDs should present an increase in the *band gap* in comparison to their bulk counterparts. However, we calculate the *band gap* and it does not occur. We believe that dopants act as electron receiving centers, by introducing vacancies and surface defects, generating intermediate levels between the valence band and conduction band. This mechanism promotes the separation of photo-excited e^+/h^- and improve the transfer of photo-excited charge carries to the adsorbed tetracycline, making the energy for the *band gap* decrease. Many works[34,54,105,107,123,136-138] report the decrease of *band gap* with doping and the decrease of size particle.

Thus, after 15 minutes of the adsorption process, and based on the *band gap* values the visible radiation source was turned on. The photocatalytic activity between pure and La^{3+} doped TiO_2 QDs did not present significant variation, as presented in Figure 19(b). The samples 1 and 3 mol% doped Ca^{2+} TiO_2 QDs (Figure 19(a)) presents better photocatalytic activity than pure and 5 mol% Ca^{2+} TiO_2 QDs, which leads to the conclusion that the amount of tetracycline adsorbed on the surface and the decrease of the band gap induces the photocatalysis reaction.

Figure 1916 - Adsorption and Photocatalysis of pure and (a)Ca^{2+}/(b)La^{3+} doped TiO_2 QDs
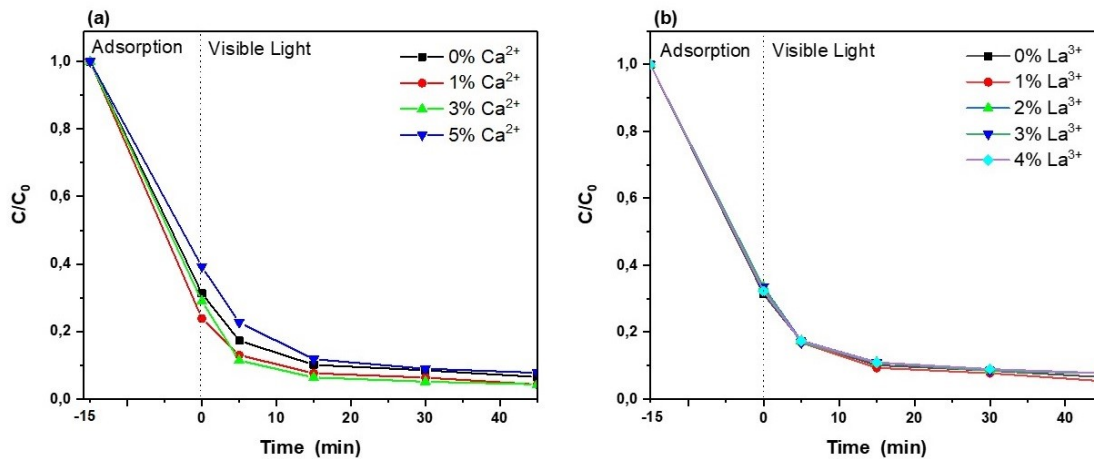
UV-vis absorption spectra, Figure 20(a), showed a broad absorption for all samples between 300 and 350 nm. The sample with 1 mol% doped Ca^{2+} TiO_2 QDs presented a redshift around 300 nm and an increased absorption intensity in the visible light range in comparison with the pristine sample, which is in accordance with the photocatalytic results that showed that doping with 1 mol% Ca^{2+} led to the highest adsorption rate. Thus, our results shows that 1 mol% Ca^{2+} shows a better photocatalytic activity, suggesting that the doping process at low concentrations of Ca^{2+} is a viable alternative to obtain a more photocatalytically efficient material.

Figure 20 - (a)Absorption (b) band gap of pure and 1, 5 mol%Ca^{2+}/ 1, 4 mol% La^{3+} doped TiO_2 QDs
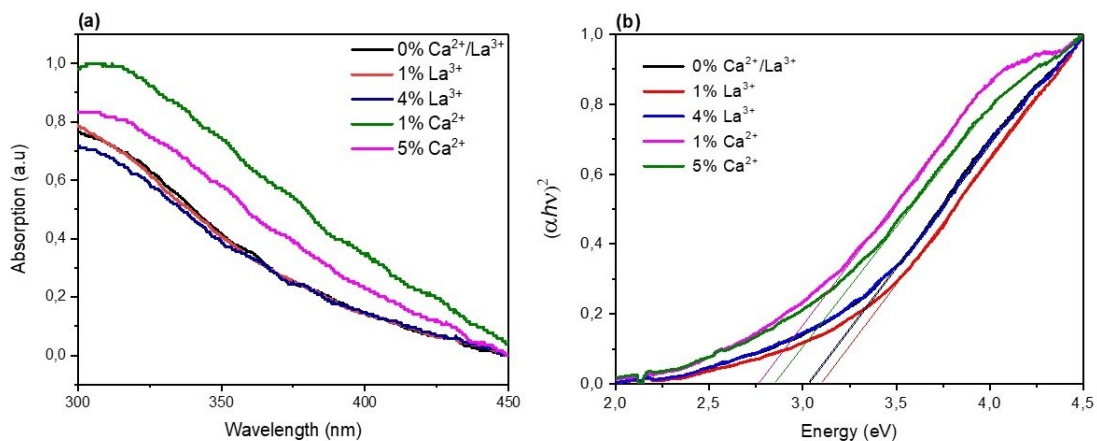
4.4 Conclusions

In summary, we present pure and Ca^{2+}/La^{3+} doped TiO_2 QDs synthesized via hydrothermal microwave treatment at 120 °C for 10 minutes. As a result, 1 mol% Ca^{2+} doped TiO_2 QDs were found as the optimized QDs for its high surface area

($412.19 \text{ m}^2.\text{g}^{-1}$) and increase of the interfacial component (64%), leading to a highly energetic and adsorptive QDs surface. In addition, it can promote electron-hole separation sample and harvest visible light because of the relatively narrow bandgap (2.72 eV), allowing for the use of visible light for degradation of 96 % of tetracycline antibiotic in 30 minutes of photocatalysis reaction. On balance, the technology used in this research provides technical support for the preparation of pure and doped TiO_2 QDs as raw material for many applications, and a scientific basis for industrial production of these photocatalysts.

Chapter 5 - Final remarks

5.1 – Conclusion of the thesis

Highly homogeneous TiO_2 QDs were synthesized and evaluated about their adsorption potential and applied as photocatalysts for the degradation of reactive red azo dye (RR141). QDs were produced by a low-energy and eco-friendly microwave-assisted method. Different microwave times (10, 20, 30, and 60 min) and temperatures (120, 140, 160, 180 ºC) were evaluated. Raman and X-ray diffraction data detected anatase as the major crystalline phase. XRD also indicated an increase in the interfacial component as the microwave temperature decreases, resulting in highly energetic surface and super adsorptive QDs. TiO_2 crystallites presented an average size of 5 to 6.2 nm as calculated from the Scherrer equation and confirmed by TEM micrographs. As a feature of the particle size reduction, the QDs synthesized by 10 min and 120 ºC presented a large specific surface area ($\sim$292 $m^2 \cdot g^{-1}$), higher interfacial component (60%), high adsorption capability and a fast ($\sim$5 min) 100% degradation of RR141, making this a promising photocatalyst techno-commercial material.

In order to study the influence of doping on the fraction of the interfacial component, TiO_2 QDs were doped with Ca^{2+} and La^{3+} varying the compositional range from 0 to 5 mol% by. As a result, the Ca^{2+}/La^{3+} doped TiO_2 QDs present crystallite size of $\sim$5 nm. The sample with 1 mol% Ca^{2+} showed a high surface area (412.19 $m^2.g^{-1}$) measured by BET analyses and an increase of the interfacial component (64 %) led to a highly energetic and adsorptive QDs surface. XDR and Raman analyses showed anatase as mainly crystal phase. The band gap of the QDs were calculated by Tauc Plout method, which reached values of 2.72 eV, permitting the use of visible light for degradation of 96 % of tetracycline antibiotic in 30 minutes of photocatalysis reaction. The QDs´s zeta-potential is about +30 mV indicating good colloidal stability.

This study has demonstrated that it is possible to produce semiconductors at lower temperatures than those stablished in the literature, keeping the crystalline structure of the material and without losing any intrinsic properties of a crystal. More than that, it was possible to deepen in other characteristics presented by the material according to temperature variations, that promoted novel properties that were explored and applied. The technique was efficient and reproducible, capable to generate

homogeneous materials with a wide range of applications in different technological areas.

5.2 – Suggestion for future works

Considering the obtained results in the present work and considering its remarkable scientific contributions, a few suggestions can be highlighted as interesting possibilities for future works applying TiO_2 QDs:

- Perform TiO_2 QD syntheses at temperatures below 120°C to analyze whether the interfacial component fraction increases and improves the adsorption property;

- Use other dopants to compare structural, morphological, thermodynamic and electronic properties;

- Use proportions below 1 mol % in doping, as the best result was with the mol% 1 Ca^{2+} sample;

- Use more refined techniques to analyze the influence of the interfacial component, such as Transmission Electron Microscopy (TEM 200 Kv);

- Analyze the doped samples for the composition and chemical states of atoms on the surface of the photocatalysts using X-Ray Photoelectron Spectroscopy (XPS);

- Determine the surface excess of dopant using the superficial lixiviation technique;

- Apply samples in sintering processes due to its large fraction of interfacial component.

References

1.   Taghipour S, Hosseini SM, Ataie-Ashtiani B. Engineering nanomaterials for water and wastewater treatment: Review of classifications, properties and applications. *New Journal of Chemistry.* 2019;43(21):7902–7927.

2.   Archana T, Vijayakumar K, Arivanandhan M, Jayavel R. TiO_2 nanostructures with controlled morphology for improved electrical properties of photoanodes and quantum dot sensitized solar cell characteristics. *Surface Interfaces.* 2019;17:11.

3.   Swamy V, Gale JD, Dubrovinsky LS. Atomistic simulation of the crystal structures and bulk moduli of TiO_2. *polymorphs.* 2000

4.   Zhao Y, Li C, Liu X, Gu F, Jiang H, Shao W, Zhang L, He Y. Synthesis and optical properties of TiO_2 nanoparticles. *Materials Letters.* 2007;61(1):79–83.

5.   Zhu T, Gao SP. The stability, electronic structure, and optical property of TiO_2 polymorphs. *Journal of Physical Chemistry C.* 2014;118(21):11385–11396.

6.   Thompson TL, Yates JT. Surface science studies of the photoactivation of TiO_2-New photochemical processes. *Chemical Reviews.* 2006;106(10):4428–4453.

7.   Etacheri V, di Valentin C, Schneider J, Bahnemann D, Pillai SC. Visible-light activation of TiO_2 photocatalysts: Advances in theory and experiments. *Journal of Photochemistry and Photobiology C: Photochemistry Reviews.* 2015;25:1–29.

8.   Feng M, Zhao J, Huang T, Zhu X, Petek H. The electronic properties of superatom states of hollow molecules. *Accounts of Chemical Research.* 2011;*44*(5):360–368.

9.   Atkins PW, PAULA J. Físico-química 2. 8. ed. Rio de Janeiro: LTC, 2008.

10.   Paidi VK, Lee BH, Ahn D, Kim KJ, Kim Y, Hyeon T, Lee KS. Oxygen-Vacancy-Driven Orbital Reconstruction at the Surface of TiO_2 Core-Shell Nanostructures. *Nano Letters.* 2021;*21*(19):7953–7959.

11.   Zhao X, Zhao Q, Yu J, Liu B. Development of multifunctional photoactive self-cleaning glasses. *Journal of Non-Crystalline Solids.* 2008;*354*(12–13):1424–1430.

12.   Fujishima A. TiO_2 photoelectrochemistry and photocataysis. 2001; *213*(1998):8656.

13.   Fujishima A, Rao TN, Tryk DA. Titanium dioxide photocatalysis. *Journal of Photochemistry and Photobiology C: Photochemistry Reviews.* 2000;*1*(1):1–21.

14.   Gandelman H, da Silva AL, Caliman LB, Gouvêa D. Surface and grain boundary excess of ZnO-doped TiO_2 anatase nanopowders. *Ceramics International.* 2018;*44*(10):11390–11396.

15.   Zhang R, Zhao J, Yang Y, Lu Z, Shi W. Understanding electronic and optical properties of La and Mn co-doped anatase TiO$_2$. *Computational Condensed Matter*. 2016;*6*: 5–17.

16.   Ahmed MH, Keyes TE, Byrne JA, Blackledge CW, Hamilton JW. Adsorption and photocatalytic degradation of human serum albumin on TiO$_2$ and Ag-TiO$_2$ films. *Journal of Photochemistry and Photobiology A: Chemistry*. 2011;*222*(1),123–131.

17.   Araña J, Doña-Rodríguez JM, Portillo-Carrizo D, Fernández-Rodríguez C, Pérez-Peña J, González Díaz O, Navío JA, Macías M. Photocatalytic degradation of phenolic compounds with new TiO$_2$ catalysts. *Applied Catalysis B: Environmental*. 2010;100(1–2):346–354.

18.   Araujo FP, Honorio LMC, Sá I L, Trigueiro P, Almeida LC, Fechine PBA, Santos FEP, Peña-Garcia R, Silva-Filho EC, Osajima JA. New composite TiO$_2$/naturals gums for high efficiency in photodiscoloration process. *Ceramics International*. 2020.

19.   Ghosh D, Ivanov SA, Tretiak S, Ghosh D. Structural Dynamics and Electronic Properties of Semiconductor Quantum Dots: Computational Insights. *Chemistry of Materials*. 2021.

20.   Wang C, Liu H, Qu Y. TiO$_2$-based photocatalytic process for purification of polluted water: Bridging fundamentals to applications. *Journal of Nanomaterials*. 2013.

21.   Du J, Zhang B, Li J, Lai B. Decontamination of heavy metal complexes by advanced oxidation processes: A review. *Chinese Chemical Letters.* 2020.

22.   Hassaan MA, Nemr Ael. Advanced Oxidation Processes for Textile Wastewater Treatment. *International Journal of Photochemistry and Photobiology*. 2017;*2*(3):85–93.

23.   Selvaraj V, Swarna Karthika T, Mansiya C, Alagar M. An over review on recently developed techniques, mechanisms and intermediate involved in the advanced azo dye degradation for industrial applications. *Journal of Molecular Structure*. 2021;*1224*.

24.   Shalimar S. Borgesa, Leandro P. S. Xavierb, A. C. da S. e S. F. de A. Imobilização de dióxido de titânio em diferentes materiais suporte para o emprego em fotocatálise heterogênea. *Quim. Nova*. 2016:1–9.

25.   Fujishima K, Honda A. *Electrochemical Photolysis of Water at a Semiconductor Electrode*. 1972;*238*, 37.

26.   Ikram M, Rashid M, Haider A, Naz S, Haider J, Raza A, Ansar MT, Uddin MK, Ali NM, Ahmed SS, Imran M, Dilpazir S, Khan Q, Maqbool M. A review of photocatalytic characterization, and environmental cleaning, of metal oxide nanostructured materials. *Sustainable Materials and Technologies*. 2021;30.

27.   Bagheri S, Termehyousefi A, Do TO. Photocatalytic pathway toward degradation of environmental pharmaceutical pollutants: Structure, kinetics and mechanism approach. *Catal Sci Technol.* 2017;7:4548-4569.

28.   Turchi CS. Photocatalytic Degradation of Organic Water Contaminants: Mechanisms Involving Hydroxyl. Radical Attack. 1990;*192*:178–192.

29.   Parveen S, Paul KK, Giri PK. tum dots confined in a mesoporous TiO_2 template grown by rapid thermal annealing High photoluminescence yield from organometal halide perovskite quan. *Aip conference proceedings.* 2019;*2082*:1–5.

30.   Jin J, Zhao L, Liu Y, Gao S, Yu X, Xiong Y. Double-layer TiO_2 inverse opal-based quantum dot-sensitized solar cells. *J Solid State Electrochem*. 2021;25:291–299.

31.   Zhao F, Ma R, Jiang Y. Strong efficiency improvement in dye-sensitized solar cells by novel multi-dimensional TiO_2 photoelectrode. *Appl Surf Sci.* 2018;434:11–15.

32.   Thao DN, Bao LTN. Quantum beat of excitons in spherical semiconductor quantum dots. *Superlattice Microst* 2020;146:106675.

33.   Bernstein, J. (2018). Advanced Quantum Mechanics. In *A Bouquet of Dyson*.

34.   Liu J, Nie Y, Xue W, Wu L, Jin H, Jin G, Zhai Z, Fu C. Size effects on structural and optical properties of tin oxide quantum dots with enhanced quantum confinement. 2020; 9:8020–8028.

35.   Venkatasubbu GD, Ramakrishnan V, Sasirekha V, Ramasamy S, Kumar J. Influence of particle size on the phonon confinement of TiO_2 nanoparticles. *Journal of Experimental Nanoscience*, 2014*9;*(7):661–668.

36.   Jing L, Ding K, Kershaw SV, Kempson IM, Rogach AL, Gao M. Magnetically Engineered Semiconductor Quantum Dots as Multimodal Imaging Probes. *Advanced Materials*. 2014;*26*(37):6367–6386.

37.   Jouyandeh M, Mousavi Khadem S, Habibzadeh S, Esmaeili A, Abida O, Vatanpour V, Rabiee N, Bagherzadeh M, Iravani S, Reza Saeb M, Varma RS. Quantum dots for photocatalysis: synthesis and environmental applications. *Green Chemistry* 2021;23(14): 4931–4954).

38.   Khordad R, Bahramiyan H. Impurity position effect on optical properties of various quantum dots. *Physica E Low Dimens Syst Nanostruct*. 2015;66:107-115.

39.   Gleiter H. Nanostructured materials: state of the art and perspectives. *Nanostructured Materials*. 1995;*6*(1–4):3–14.

40.   Gleiter H. Nanostructured materials: basic concepts and microstructure. *Acta Materialia*, 2000;*48*(1):1–29.

41.	Zubko P, Gariglio S, Gabay M, Ghosez P, Triscone JM. Interface physics in complex oxide heterostructures. *Annual Review of Condensed Matter Physics*. 2011;*2*(1):141–165.

42.	Crocker AG, Elvidge AM, Flewitt PEJ. Structure and properties of polycrystalline materials. *Physica Scripta*, 1987;(T19B):344–349.
43.	N K M'Sirdi, J. Z. (1982). Filtres En Peigne Adaptatifs Pour L'Estimation Des Composantes Harmoniques D'Un Signal. *J. Phys. Colloques*. 2015;43:5491-5503.

44.	Lewis TJ. Interfaces are the Dominant Feature of Dielectrics at the Nanometric Level. *IEEE Transactions on Dielectrics and Electrical Insulation*. 2004;11(5):739 - 753.

45.	Borges, Z. v., Poffo, C. M., de Lima, J. C., de Souza, S. M., Trichês, D. M., Nogueira, T. P. O., Manzato, L., & de Biasi, R. S. (2016). Study of structural, optical and thermal properties of nanostructured SnSe2 prepared by mechanical alloying. *Materials Chemistry and Physics*, *169*, 47–54.

46.	Gleiter, H. Our thoughts are ours, their ends none of our own: Are there ways to synthesize materials beyond the limitations of today? *Acta Materialia*. 2008*56*(19):5875–5893.

47.	Teh CM, Mohamed AR. Roles of titanium dioxide and ion-doped titanium dioxide on photocatalytic degradation of organic pollutants (phenolic compounds and dyes) in aqueous solutions: A review. *Journal of Alloys and Compounds*. 2011;509(5):1648–1660).

48.	Guo Q, Zhou C, Ma Z, Ren Z, Fan H, Yang X. Fundamental Processes in Surface Photocatalysis on TiO_2. 2016;361–416.

49.	Nazir B, Rehman U ur, Arshad S, Arshad MI, Sabir N, Arshad Javid M, Iqbal F, Ajaz un Nabi M. Enhanced photo-absorption of anatase TiO_2 with Ni and Eu doping: A first principle study. *Materials Today: Proceedings*. 2020; 0–4.

50.	Wang R, An S, Zhang J, Song J, Wang F. Existence form of lathanum and its improving mechanism of visible-light-driven La-F co-doped TiO_2. *Journal of Rare Earths*, 2020;*38*(1):39–45.

51.	Wen C, Deng H, Tian JY, Zhang JM. Photocatalytic activity enhancing for TiO_2 photocatalyst by doping with La. *Transactions of Nonferrous Metals Society of China* 2006;16:4–7.

52.	Chen T, Foo C, Tsang SCE. Interstitial and substitutional light elements in transition metals for heterogeneous catalysis. In *Chemical Science*. 2021;12(2):517–532.

53.	Toghan A, Modwi A, Khairy M, Taha KK. Influence of TiO_2 concentration on the characteristics of ZnO nanoparticles fabricated via sonication assisted with gelatin. *Chemical Physics*. 2021;551.

54.   Trochowski M, Kobielusz M, Mróz K, Surówka M, Hämäläïnen J, Iivonen T, Leskelä M, Macyk W. How insignificant modifications of photocatalysts can significantly change their photocatalytic activity. *Journal of Materials Chemistry A*. 2019;*7*(43):25142–25154.

55.   Huang Y, Cao JJ, Kang F, You SJ, Chang CW, Wang YF. High selectivity of visible-light-driven la-doped TiO_2 photocatalysts for NO removal. *Aerosol and Air Quality Research*. 2017;17(10):2555–2565.

56.   Nešić J, Manojlović DD, Andelković I, Dojčinović BP, Vulić PJ, Krstić J, Roglić GM. Preparation, characterization and photocatalytic activity of lanthanum and vanadium co-doped mesoporous TiO_2 for azo-dye degradation. *Journal of Molecular Catalysis A: Chemical*. 2013;378:67–75.

57.   Suwarnkar MB, Dhabbe RS, Kadam AN, Garadkar KM. Enhanced photocatalytic activity of Ag doped TiO_2 nanoparticles synthesized by a microwave assisted method. *Ceramics International*. 2014;40(4):5489–5496.

58.   da Silva AL, Muche DNF, Caliman LB, Bettini J, Castro RHR, Navrotsky A, Gouvêa D. TiO_2 Surface Engineering to Improve Nanostability: The Role of Interface Segregation. *Journal of Physical Chemistry C*. 2019;*123*(8):4949–4960.

59.   Castro RHR. Interfacial energies in nanocrystalline complex oxides. *Current Opinion in Solid State and Materials Science*. 2021;*25*(3).

60.   Da Silva AL, Wu L, Caliman LB, Castro RHR, Navrotsky A, Gouvêa D. Energetics of CO_2 and H_2O adsorption on alkaline earth metal doped TiO_2. Phys Chem Chem Phys 2020;22:15600-15607.

61.   Rafieh AI, Ekanayake P, Nakajima H, Mahadi AH, Abu M, Don MF, Lim CM. Enhanced N719 Dye Adsorption onto Ca and La Doped Mesoporous TiO_2 Anodes for Dye-Sensitized Solar Cells. *Journal of Electronic Materials*. 2021;*50*(10):5788–5795.

62.   Gandelman H, da Silva AL, Ramos B, Gouvêa D. Interface excess on Sb-doped TiO_2 photocatalysts and its influence on photocatalytic activity. *Ceramics International*. 2021;47(1):619–625.

63.   Baldassari S, Komarneni S, Marian E, Villa C. Rapid microwave-hydrothermal synthesis of anatase form of titanium dioxide. *Journal of the American Ceramic Society*. 2005;88(11):3238–3240.

64.   Chen P, Peng Jde, Liao CH, Shen PS, Kuo PL. Microwave-assisted hydrothermal synthesis of TiO_2 spheres with efficient photovoltaic performance for dye-sensitized solar cells. *Journal of Nanoparticle Research*. 2013;*15*(3).

65.   Falk G, Borlaf M, Fariñas JC. Microwave-assisted synthesis of Nb_2O_5 for photocatalytic application of nanopowders and thin films. *J. Mater. Res*. 2017;32(17):71–3278.

66.   Ferrari AM, Emilia R, Grippo C, Marian E, Villa C. Conventional and Microwave-Hydrothermal Synthesis of TiO$_2$ Nanopowders. *J. Am. Ceram. Soc.* 2005;88(9):2639–2641.

67.   Wu X, Jiang Q, Ma Z. Synthesis of titania nanotubes by microwave irradiation. *Solid State Communications*. 2005;*136*:513–517.

68.   Lau CC, Bayazit MK, Reardon PJ, Tang J. Microwave intensified synthesis: batch and flow chemistry. *Chem Rec*. 2019;19:172-187.

69.   Conner WC, Tompsett GA. How could and do microwaves influence chemistry at interfaces? *Am J Phys Chem*. 2008;112:2110-2118.

70.   Pauzi N, Mat Zain N, Ahmad Yusof NA. Microwave-Assisted Synthesis for Environmentally ZnO Nanoparticle Synthesis. *Lecture Notes in Electrical Engineering*. 2019;538.

71.   Rathi AK, Gawande MB, Zboril R, Varm, S. Microwave-assisted synthesis - Catalytic applications in aqueous media. *Coordination Chemistry Reviews*. 2015;291:68–94.

72.   Zhu YJ, Chen F. Microwave-assisted preparation of inorganic nanostructures in a liquid phase. *Chem Rev*. 2014;114:6462-6555.

73.   El-Nabulsi RA. A new approach to the schrodinger equation with position-dependent mass and its implications in quantum dots and semiconductors. *J Phys Chem Solids* 2020;140:109384.

74.   Ramachandran R, Jung D. Spokoyny AM Cross-linking dots on metal oxides. *NPG Asia Mater*, 2019;11:1-4.

75.   Wang G, Yang Y, Han D, Li Y Oxygen defective metal oxides for energy conversion and storage. *Nano Today*. 2017;13:23-39.

76.   Xiong J, Di J, Xia J, Zhu W, Li H. Surface Defect Engineering in 2D Nanomaterials for Photocatalysis. *Adv Funct Mate*r 2018;23:19.

77.   Concina I, Vomiero. A Metal oxide semiconductors for dye-and quantum-dot-sensitized solar cells. *Small*. 2015;11:1744-1774.

78.   Wang X, Xia R, Muhire E, Jiang S, Huo X, Gao M. Performance of TiO$_2$ nanosheets through constructing TiO$_2$/TiO$_2$ quantum dots homojunction. *Appl Surf Sci*. 2018;459:9-15.

79.   Javed S, Islam M, Mujahid M. Synthesis and characterization of TiO$_2$ Quantum Dots by sol-gel reflux condensation method. *Ceram Int*. 2020;45:2676-2679.

80.   Zhu X, Cai D, Cui Z, Wang Q, Zhan H. Embedded ZnO nanoparticles in N-doped carbon nanoplate arrays grown on N-doped carbon paper as low-cost and lightweight electrodes for high-performance lithium storage. *Ceram. Int*. 2020;46:17767–17775.

81.	Caliman LB, Muche D, Silva A, Ospina RCA, Machado IF, Castro RHR, Gouvêa D. Effect of segregation on particle size stability and SPS sintering of Li_2O-Doped magnesium aluminate spinel. *J Eur Ceram Soc*. 2019;39:3213-3220.

82.	Zhao F, Ma R, Jiang Y. Strong efficiency improvement in dye-sensitized solar cells by novel multi-dimensional TiO_2 photoelectrode. *Appl Surf Sci*. 2018;434:11–15.

83.	Wu DP, Zhang S, Jiang SW, He JJ, Jiang K. Anatase TiO_2 hierarchical structures composed of ultra-thin nano-sheets exposing high percentage {001} facets and their application in quantum-dot sensitized solar cells. *J Alloys Compd*. 2015;624:94–99.

84.	Xu Y, Wu W, Rao H, Chen H, Kuang D, Su C. CdS/CdSe co-sensitized TiO_2 nanowire-coated hollow Spheres exceeding 6% photovoltaic performance. *Nano Energy*. 2015;11:621–630.

85.	Zhang XL, Lin Y, Wu J H, Jing J, Fang BP. Improved performance of CdSe/CdS/PbS co-sensitized solar cell with double-layered TiO_2 films as photoanode. *Opt Commun*. 2017;395:117–121.

86.	Lu YB, Li L, Su SC, Chen YJ, Song YL, Jiao SJ A novel TiO_2 nanostructure as photoanode for highly efficient CdSe quantum dot-sensitized solar cells. *RSC Adv*. 2017;7: 9795–9802.

87.	Veerathangam K, Pandian MS, Ramasamy P. Size-dependent photovoltaic performance of cadmium sulfide (CdS) quantum dots for solar cell applications. *J Alloys Compd*. 2018;735:202–208.

88.	Kim HJ, Xu GC, Gopi CVVM, Seo H, Venkata-Haritha M, Shiratani M. Enhanced light harvesting and charge recombination control with TiO_2/PbCdS/CdS based quantum dot-sensitized solar cells. *J Electroanal Chem*. 2017;788:131–136.

89.	Yuan BL, Gao QQ, Zhang XY, Duan LF, Chen L, Mao Z, Li XS, Lü W. Reduced graphene oxide (RGO)/Cu_2S composite as catalytic counter electrode for quantum dot-sensitized solar cells. *Electrochim Acta*. 2018;277:50–58.

90.	Freyria F.S. Colloidal Semiconductor Nanocrystals for Artificial Photosynthesis. In: Piumetti M., Bensaid S. (eds) Nanostructured Catalysts for Environmental Applications. Springer, Cham. 2021.

91.	Liu J, Zhang Q, Tian X, Hong Y, Nie Y, Su N, Jin G, Zhai Z, Fu. Highly efficient photocatalytic degradation of oil pollutants by oxygen deficient SnO_2 quantum dots for water remediation. *Chem Eng J C*. 2021;404:127146.

92.	Dąbrowski A. Adsorption - From theory to practice**.** Adv. *Colloid Interface Sci***.** 2001;93:135-224.

93.   Akram M, Hussain R, Butt FK, Latif M. Study of the effect of microwave holding time on the physicochemical properties of titanium oxide. *Mater Res Express*. 2019;6:085041.

94.   Danish R, Ahmed F, Koo B. Rapid synthesis of high surface anatase Titanium Oxide quantum dots. *Ceram Int*. 2014;80:12675-880.

95.   Sharma S, Umar A, Mehta SK, Ibhadon A, Sheikh SK. Solar light-driven photocatalytic degradation of levofloxacin using TiO_2/carbon-dot nanocomposites. *New J Chem.* 2018;42:7445-7456.

96.   Kolahalam LA, Kasi VIV, Diwakar BS, Govindh B, Reddy V, Murthly YLN. Review on nanomaterials: Synthesis and applications. *Mater Today Proc*. 2019;18:2182-2190.

97.   Falk GS, Borlaf M, López-Muñoz MJ, Rodrigues Neto JB, Moreno R. Microwave-assisted synthesis of TiO_2 nanoparticles: photocatalytic activity of powders and thin films. *J Nanopart Res*. 2018;0:23.

98.   Vorokh A. Scherrer formula: estimation of error in determining small nanoparticle size. *Nanosyst Phys Chem Math*. 2018;9:364-369.

99.   Araujo FP, Honorio LMC, Sá IL, Trigueiro P, Almeida LC, Fechine PBA, Santos FEP, Peña-Garcia R, Silva-Filho EC, Osajima JA. New composite TiO_2/naturals gums for high efficiency in photodiscoloration process. *Ceram Int.* 2020;46:15534-15543.

100.   Kansal SK, Kundu P, Sood S, Lamba R, Umar A, Mehta SK. Photocatalytic degradation of the antibiotic levofloxacin using highly crystalline TiO_2 nanoparticles. *New J Chem*. 2014;38:3220-3226.

101.   Sheikh M, Naikoo GA, Thomas M, Bano M, Khan F. Solar-assisted photocatalytic reduction of methyl orange azo dye over porous TiO_2 nanostructures. *New J Chem*. 2016;40:5483-5494.

102.   Chen X, Mao SS. Titanium dioxide nanomaterials: synthesis, properties, modifications and applications. *Chem Rev*. 2007;107:2891–2959.

103.   Luque R, Prinsen P. Introduction to Nanocatalysts, in: Luque R, Prinsen P, Nanoparticle Design and Characterization for Catalytic Applications in Sustainable *Chemistry*. 2019:1-36.

104.   Rajabi HR. Photocatalytic activity of quantum dots, in: Semiconductor Photocatalysis. *Materials, Mechanisms, and Applications*, InTech, Croatia. 2016:471-489.

105.   Bi X, Du G, Kalam A, Sun D, Yu Y, Su Q, Xu B, Al-Sehemi AG. Tuning oxygen vacancy content in TiO_2 nanoparticles to enhance the photocatalytic performance. *Chemical Engineering Science*. 2021;*234*.
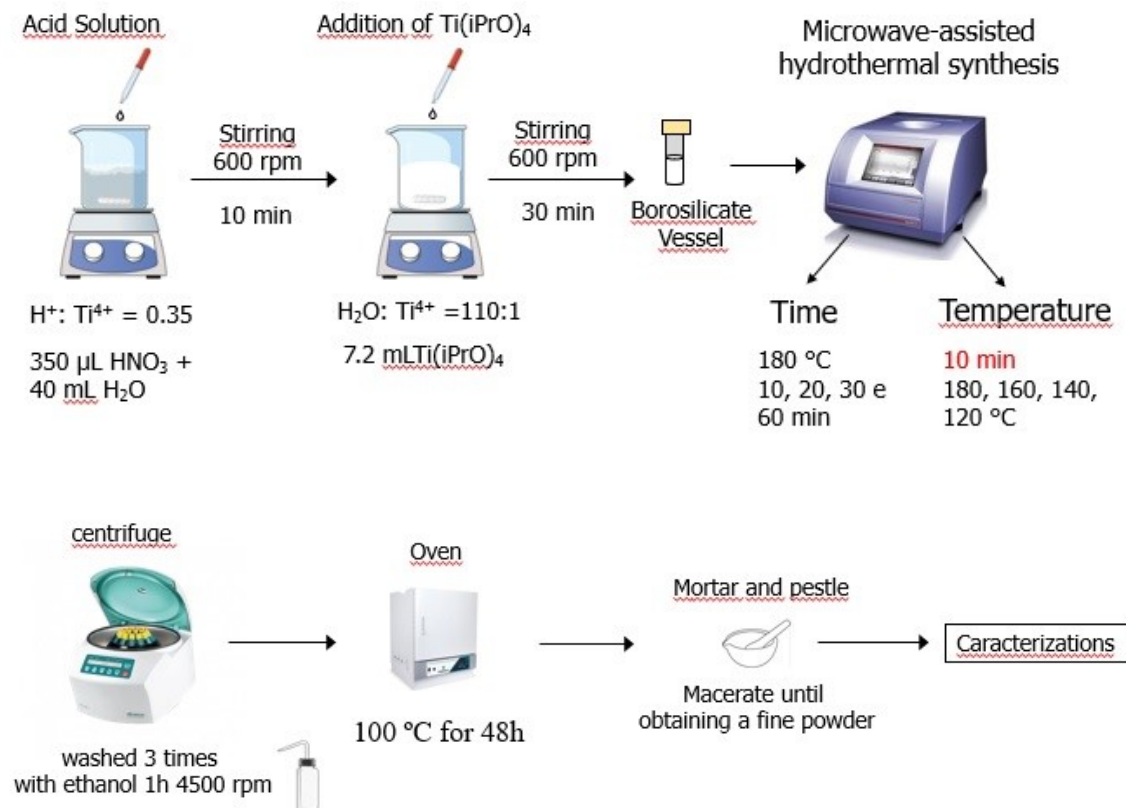
106.   Li D, Song H, Men X, Shen T, Sun J, Han W, Wang X. Effects of particle size on the structure and photocatalytic performance by alkali-treated TiO$_2$. *Nanomaterials*. 2020;*10*(3):

107.   Wang L, Cai Y, Liu B, Dong. A facile synthesis of brown anatase TiO$_2$ rich in oxygen vacancies and its visible light photocatalytic property. *Solid State Ionics*. 2021;*361*.

108.   Stern EA, Siegel RW, Newville M, Sanders PG, Haskel D. Are Nanophase Grain Boundaries Anomalous? *Phys. Rev. Lett*. 1005;75(21):3874-3877.

109.   Galstyan V. Quantum dots: Perspectives in next-generation chemical gas sensors – A review. *Analytica Chimica Acta*. 2021;1152

110.   Kumbhakar P, Roy Karmakar A, Das GP, Chakrabort J, Tiwary C Kumbhakar P. Reversible temperature-dependent photoluminescence in semiconductor quantum dots for the development of a smartphone-based optical thermometer. *Nanoscale*. 2021;*13*(5):2946–2954.

111.   Wang G, Wang F, Liu , Li M, Xie M, Yang Z, Xiang Y, Lv S, Han W. Construction of heterojuncted photocatalyst with TiO$_2$ quantum dots and graphene oxide nanosheets for highly efficient photocatalysis. *Scripta Materialia*. 2021;*199*.

112.   Sharma K, Raizada P, Hasija V, Singh P, Bajpai A, Nguyen VH, Rangabhashiyam S, Kumar P, Nadda AK, Kim SY, Varma RS, Le TTN, Le Q. ZnS-based quantum dots as photocatalysts for water purification. *Journal of Water Process Engineering* 2021;43.

113.   Li G, Wang BD, Sun Q, Xu WQ, Han, YF. Visible-Light Photocatalytic Activity of Fe and/or Ni Doped Ilmenite Derived-Titanium Dioxide Nanoparticles. *Journal of Nanoscience and Nanotechnology*. 2019;*19*(6)3343–3355.

114.   Divakaran K, Baishnisha A, Balakumar V, Perumal KN, Meenakshi C, Kannan, RS. Photocatalytic degradation of tetracycline under visible light using TiO$_2$@sulfur doped carbon nitride nanocomposite synthesized via in-situ method. *Journal of Environmental Chemical Engineering*. 2021;*9*(4).

115.   Huang J, Dou L, Li J, Zhong J, Wang T. Excellent visible light responsive photocatalytic behavior of N-doped TiO$_2$ toward decontamination of organic pollutants. *Journal of Hazardous Materials*. 2021;*403*.

116.   Karuppasamy P, Ramzan Nilofar Nisha N, Pugazhendhi A, Kandasamy S, Pitchaimuthu S. An investigation of transition metal doped TiO$_2$ photocatalysts for the enhanced photocatalytic decoloration of methylene blue dye under visible light irradiation. *Journal of Environmental Chemical Engineering*. 2021;*9*(4).

117.   Acosta-Silva YJ, Méndez-López A, de Moure-Flores F, Tomás S, Lozada-Morales R, Meléndez-Lira M, Zelaya-Angel O. Characterization of substitutional and interstitial Eu^{+3}-positions in CdS lattice. *Materials Chemistry and Physics*. 2021;*257*. h
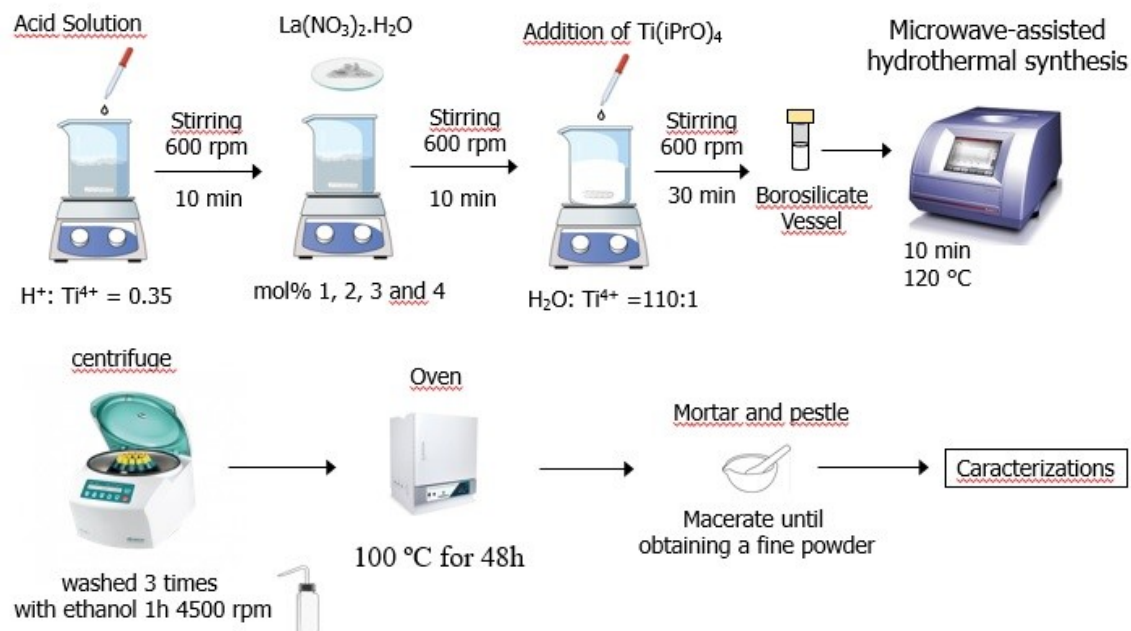
118.   Chen T, Foo C, Tsang SCE. Interstitial and substitutional light elements in transition metals for heterogeneous catalysis. *Chemical Science*. 2021;12(2):517–532.

119.   Wang Y, Wang X, Li L, Wu Y, Yu Q. An experimental and theoretical study on the photocatalytic antibacterial activity of boron-doped TiO_2 nanoparticles. *Ceramics International*, 2021;48:604-614.

120.   Frizzo MS, Betega K, Poffo C, Falk, GS, Hotza D, Rodrigues Neto JB. Highly enhanced adsorption and photocatalytic performance of TiO_2 quantum dots synthesized by microwaves for degradation of reactive red azo dye. *Journal of Nanoparticle Research*, 2021;23(5)113.

121.   Bernardes AA, Caliman LB, da Silva A, Bettini J, Guimarães KL, Gouvea D. Li_2O-doped $MgAl_2O_4$ nanopowders: Energetics of interface segregation. *Journal of the American Ceramic Society*. 2020;*103*(4):2835–2844.

122.   de Oliveira RAMP, da Silva AL, Caliman LB, Gouvêa D. Interface excess on Li_2O-doped γ-Al_2O_3 nanoparticles. *Ceramics International*. 2020;*46*:10555–10560.

123.   Caligulu U, Darcan N, Kejanli H. Surface morphology and optical properties of Ca and Mn doped TiO_2 nano-structured thin films. *Engineering Science and Technology, an International Journal*. 2021.

124.   Castro Y, Arconada N, Durán A. Synthesis and photocatalytic characterisation of mesoporous TiO_2 films doped with Ca, W and N. *Boletin de La Sociedad Espanola de Ceramica y Vidrio*. 2015;*54*(1):11–20.

125.   Colpani GL, Santos VF, Zeferino RCF, Zanetti M, Mell JMM, Silva LL, Padoin, N, Moreira R de FPM, Fiori MA, Soares C. Propranolol hydrochloride degradation using La@TiO_2 functionalized with CMCD. *Journal of Rare Earths* .2021.

126.   Bhandarkar SA, Prathvi Kompa A, Murari MS, Kekuda D, Mohan RK. Investigation of structural and optical properties of spin coated TiO2:Mn thin films. *Optical Materials*. 2021;*118*.

127.   Palomino-Merino R, Trejo-Garcia P, Portillo-Moreno O, Jiménez-Sandoval S, Tomás SA, Zelaya-Angel O, Lozada-Morales R, Castaño VM. Red shifts of the $E_{g(1)}$ Raman mode of nanocrystalline TiO2:Er monoliths grown by sol-gel process. *Optical Materials*. 2015;*46*:345–349.

128.   Boyd RW. Stimulated Raman Scattering and Stimulated Rayleigh-Wing Scattering. In *Nonlinear Optics.* 2020;459–493.

129.   Korepanov VI, Chan SY, Hsu HC, Hamaguchi HO. Phonon confinement and size effect in Raman spectra of ZnO nanoparticles. *Heliyon*. 2019;*5*(2):1–14.

130.   Akshay VR, Arun B, Mandal G, Chanda A, Vasundhara M. Significant reduction in the optical band-gap and defect assisted magnetic response in Fe-doped anatase TiO_2 nanocrystals as dilute magnetic semiconductors. *New Journal of Chemistry*, 2019;*43*(15):6048–6062.

131.   Bai L, Lin Z, Wen M, Dong H, Liu Z, Chen S, Wu F. Vacancies inducing electronic and optical properties in 2D ZnO:Be/Mg. *Physica B: Condensed Matter*. 2019;*555*:47–52.

132.   Hess C. New advances in using Raman spectroscopy for the characterization of catalysts and catalytic reactions. *Chemical Society Reviews*. 2021;*50*(5):3519–3564.

133.   Kumaravel V, Rhatigan S, Mathew S, Michel MC, Bartlett J, Nolan M, Hinder SJ, Gascó A, Ruiz-Palomar C, Hermosilla D, Pillai SC Mo doped TiO_2: impact on oxygen vacancies, anatase phase stability and photocatalytic activity. *Journal of Physics: Materials*. 2020;*3*(2):025008.

134.   Singh J, Sharma S, Sharma S, Singh RC. Effect of tungsten doping on structural and optical properties of rutile TiO_2 and band gap narrowing. *Optik*. 2019;*182*:538–547.

135.   Wang Q, Zhang S, He H, Xie C, Tang Y, He C, Shao M, Wang H. Oxygen Vacancy Engineering in Titanium Dioxide for Sodium Storage. *Chemistry - An Asian Journal*, 2021;*16*(1):3–19.

136.   Ghorashi MS, Madaah Hosseini HR, Mohajerani E, Pedroni M, Taheri Ghahrizjani R. Enhanced TiO_2 Broadband Photocatalytic Activity Based on Very Small Upconversion Nanosystems. *Journal of Physical Chemistry C*. 2021;*125*(25):13788–13801.

137.   Chen S, Xiao Y, Wang Y, Hu Z, Zhao H, Xie W. A facile approach to prepare black TiO_2 with oxygen vacancy for enhancing photocatalytic activity. *Nanomaterials*. 2018;*8*(4).

138.   Wang H, Sun T, Xu N, Zhou Q, Chan, L. 2D sodium titanate nanosheet encapsulated Ag_2O-TiO_2 p-n heterojunction photocatalyst: Improving photocatalytic activity by the enhanced adsorption capacity. *Ceramics International*, 2021;*47*(4):4905–4913.

139.   Tauc J, Grigorovici R, Vancu A. Optical Properties and Electronic Structure of Ge Optical Properties and Electronic Structure of Amorphous Germanium. *phys. stat. sol* 1966;15:627-637.

140.   Teh CM, Mohamed AR. Roles of titanium dioxide and ion-doped titanium dioxide on photocatalytic degradation of organic pollutants (phenolic compounds and dyes) in aqueous solutions: A review. *Journal of Alloys and Compounds*. 2011;509(5):1648–1660).

141.   De LGJ, Blasse G. The Observation of Exciton Emission from Rutile Single Crystals. *Journal of solid state chemistry*. 1986;61.

142.   Tai JY, Leong KH, Saravanan P, Aziz AA, Sim LC. Dopant-free oxygen-rich titanium dioxide: LED light-induced photocatalysis and mechanism insight. *Journal of Materials Science* 2017;*52*(19):11630–11642.

143.   Abazović ND, Čomor MI, Dramićanin MD, Jovanović DJ, Ahrenkiel SP, Nedeljković JM. Photoluminescence of anatase and rutile TiO_2 particles. *Journal of Physical Chemistry B*. 2006;*110*(50):25366–25370.

144.   Zenou, VY, Bakardjieva S. Microstructural analysis of undoped and moderately Sc-doped TiO_2 anatase nanoparticles using Scherrer equation and Debye function analysis. *Materials Characterization*. 2018;*144*:287–296.

145.   Li W, Yang J, Zhang J, Gao S, Luo Y, Liu M. Improve photovoltaic performance of titanium dioxide nanorods based dye-sensitized solar cells by Ca-doping. *Materials Research Bulletin*. 2014;*57*:177–183.

146.   Prabavathy N, Balasundaraprabhu R, Balaji G, Malikaramage AU, Prasanna S, Sivakumaran K, Kumara GRA, Rajapakse RMG, Velauthapillai D. Investigations on the photo catalytic activity of calcium doped TiO_2 photo electrode for enhanced efficiency of anthocyanins based dye sensitized solar cells. *Journal of Photochemistry and Photobiology A: Chemistry*. 2019;*377*:43–57.

APPENDIX A

ILLUSTRATED SCHEME OF THE EXPERIMENTAL PROCEDURE

Microwave-assisted hydrothermal synthesis of titanium dioxide quantum dots

Acid Solution

Stirring 600 rpm

10 min

H$^+$: Ti^{4+} = 0.35

350 µL HNO$_3$ + 40 mL H$_2$O

Addition of Ti(iPrO)$_4$

Stirring 600 rpm

30 min

H$_2$O: Ti^{4+} =110:1

7.2 mLTi(iPrO)$_4$

Borosilicate Vessel

Microwave-assisted hydrothermal synthesis

Time

180 °C

10, 20, 30 e 60 min

Temperature

10 min

180, 160, 140, 120 °C

centrifuge

washed 3 times with ethanol 1h 4500 rpm

Oven

100 °C for 48h

Mortar and pestle

Macerate until obtaining a fine powder

Caracterizations

Microwave-assisted hydrothermal synthesis of La³⁺ doped titanium dioxide quantum

Microwave-assisted hydrothermal synthesis of Ca²⁺ doped titanium dioxide quantum